nature communications

Article

https://doi.org/10.1038/s41467-024-54139-8

A platform for mapping reactive cysteines within the immunopeptidome

Received: 7 August 2024

Accepted: 31 October 2024

Published online: 08 November 2024

Check for updates

Chenlu Zhang[1,7], Chen Zhou[1,7], Assa Magassa[1,2], Xiaokang Jin[1], Deyu Fang[3] & Xiaoyu Zhang[1,2,4,5,6]

The major histocompatibility complex class I antigen presentation pathways play pivotal roles in orchestrating immune responses. Recent studies have begun to explore the therapeutic potential of cysteines within the immunopeptidome, such as the use of covalent ligands to generate haptenated peptide neoepitopes for immunotherapy. In this work, we report a platform for mapping reactive cysteines on MHC-I-bound peptide antigens. We develop cell-impermeable sulfonated maleimide probes capable of capturing reactive cysteines on these antigens. Using these probes in chemoproteomic experiments, we discover that cysteines on MHC-I-bound antigens exhibit various degrees of reactivity. Moreover, interferon-gamma stimulation enhances the reactivity of cysteines at position 8 of 9-mer MHC-I-bound antigens. Finally, we demonstrate that targeting reactive cysteines on MHC-I-bound antigens with a maleimide-conjugated Fc-binding cyclic peptide contributes to the induction of antibody-dependent cellular phagocytosis.

The major histocompatibility complex class I (MHC-I) antigen presentation pathways play central roles in regulating immune responses, impacting various physiological functions and disease progressions[1–3]. This essential role hinges largely on the interaction between the T-cell receptor (TCR) of cytotoxic $CD8^+$ T cells and the peptide-MHC-I (pMHC-I) complex displayed on the cell surface[4]. In the context of cancer, the identification of tumor-specific or tumor-associated antigens presented on MHC-I is fundamental for mounting an effective $CD8^+$ T cell antitumor immune response[5]. Conversely, in autoimmune disorders, autoreactive T cells evade thymic negative selection and peripheral tolerance mechanisms, leading to the attack on self-derived pMHC-I complexes in healthy tissues[6].

In human genome, approximately 262,000 cysteines are encoded and distributed within proteins from diverse classes and families[7]. The development of covalent chemical probes and drugs targeting cysteines has potential for elucidating protein functions and offering therapeutic interventions[8]. Despite this, our understanding of the functionality and reactivity of cysteines within MHC-I bound immunopeptidome has been limited. Recent studies have begun to exploit antigen cysteines for therapeutic applications. For example, introducing an engineered disulfide bond between TCR and MHC-I-bound antigens has been shown to facilitate T cell activation[9]. Additionally, employing covalent inhibitors to modify cysteines on intracellular proteins leads to the presentation of ligand-modified antigens on MHC-I[10,11]. These haptenated neoepitopes can be therapeutically exploited to recruit cytotoxic T cells through bispecific T cell engagers (BiTEs)[10,11]. Out of the over 520,000 MHC-I-associated antigens listed in The Immune Epitope Database (IEDB), approximately 20,000 antigens harbor cysteine residues. However, the extent to which these cysteines are amenable to therapeutic targeting remains an unexplored area. Here, we report a platform for mapping reactive cysteines on MHC-I-bound antigens, which enables the exploration of the targetable immunopeptidome from diverse perspectives.

[1]Department of Chemistry, Northwestern University, Evanston, IL 60208, USA. [2]Chemistry of Life Processes Institute, Northwestern University, Evanston, IL 60208, USA. [3]Department of Pathology, Northwestern University Feinberg School of Medicine, Chicago, IL 60611, USA. [4]International Institute for Nanotechnology, Northwestern University, Evanston, IL 60208, USA. [5]Robert H. Lurie Comprehensive Cancer Center, Northwestern University Feinberg School of Medicine, Chicago, IL 60611, USA. [6]Center for Human Immunobiology, Northwestern University Feinberg School of Medicine, Chicago, IL 60611, USA. [7]These authors contributed equally: Chenlu Zhang, Chen Zhou. e-mail: zhang@northwestern.edu

https://doi.org/10.1038/s41467-024-54139-8

Results

Development of cell-impermeable cysteine-reactive probes

Three key features should be considered when designing broad-spectrum probes for mapping reactive cysteines within the immunopeptidome: 1) spatial specificity: The probes remain in the extracellular space; 2) residue specificity: The probes selectively target cysteines without reacting with other amino acids; and 3) quantification capability: The unique modification generated by the probe can be quantified using various analytical techniques, including flow cytometry, fluorometric assays, and mass spectrometry (MS). Due to the oxidizing environment of the extracellular milieu, which leads to interchain disulfide bond formation among extracellular protein cysteines[12], we anticipate that cell-impermeable cysteine-reactive probes may primarily label cysteines within the immunopeptidome. In accordance with these criteria, we synthesized six probes, each incorporating one of three cysteine-reactive groups (iodoacetamide, α-chloroacetamide, and maleimide), all linked to desthiobiotin (DTB) (Fig. 1a). Among these probes, iodoacetamide-PEG-desthiobiotin (IA-DTB) and desthiobiotin iodoacetamide (DBIA) are widely used in the activity-based protein profiling (ABPP) platform for profiling protein cysteines[13,14]. To achieve spatial specificity, we introduced a negatively charged group, such as carboxyl or sulfonate, a strategy previously used to confer cell impermeability to small molecules[15].

Initially, we used flow cytometry to assess cell surface labeling by these reactivity probes. BV173 (human B cell leukemia) and MT2 (human T cell leukemia) cells were treated with the probe, followed by washing out of the free probe and subsequent incubation with streptavidin-fluorescein isothiocyanate (FITC) (Fig. 1b). As streptavidin-FITC remains impermeable to cells[16], the fluorescence measured by flow cytometry should primarily reflect extracellular cysteine labeling by the probe. The results revealed that two sulfonated maleimide probes, maleimide-sulfonate-dibenzocyclooctyne-DTB (MSD-DTB) and maleimide-sulfonate-DTB (MS-DTB), exhibited greater cell surface labeling in both BV173 and MT2 cells compared to others (Fig. 1b and Supplementary Fig. 1). To validate the specific reactivity towards cysteines by the MSD-DTB and MS-DTB probes, we incubated them with two peptides at a pH of 7.4: one containing a cysteine and the other lacking it. Liquid chromatography-mass spectrometry (LC-MS) analysis indicated that the maleimide reactive group selectively modifies cysteine residues, displaying no reactivity towards histidine and serine, and N-terminal amine (Fig. 1c and Supplementary Fig. 2a). Moreover, we incubated maleimide-sulfonate-dibenzocyclooctyne (MSD, Fig. 1d) with the same two peptides, followed by an azide-alkyne cycloaddition[17,18] with tetramethylrhodamine (TAMRA) azide, and observed labeling only on the cysteine-containing peptide (Supplementary Fig. 2b).

To validate cell impermeability of sulfonated maleimide probes, we treated HEK293T cells with MSD and a MSD derivative with a longer linker (maleimide-sulfonate-PEG4-dibenzocyclooctyne, or MSD4), followed by fluorophore conjugation through an azide-alkyne cycloaddition[17,18] and in-gel fluorescence analysis. The results

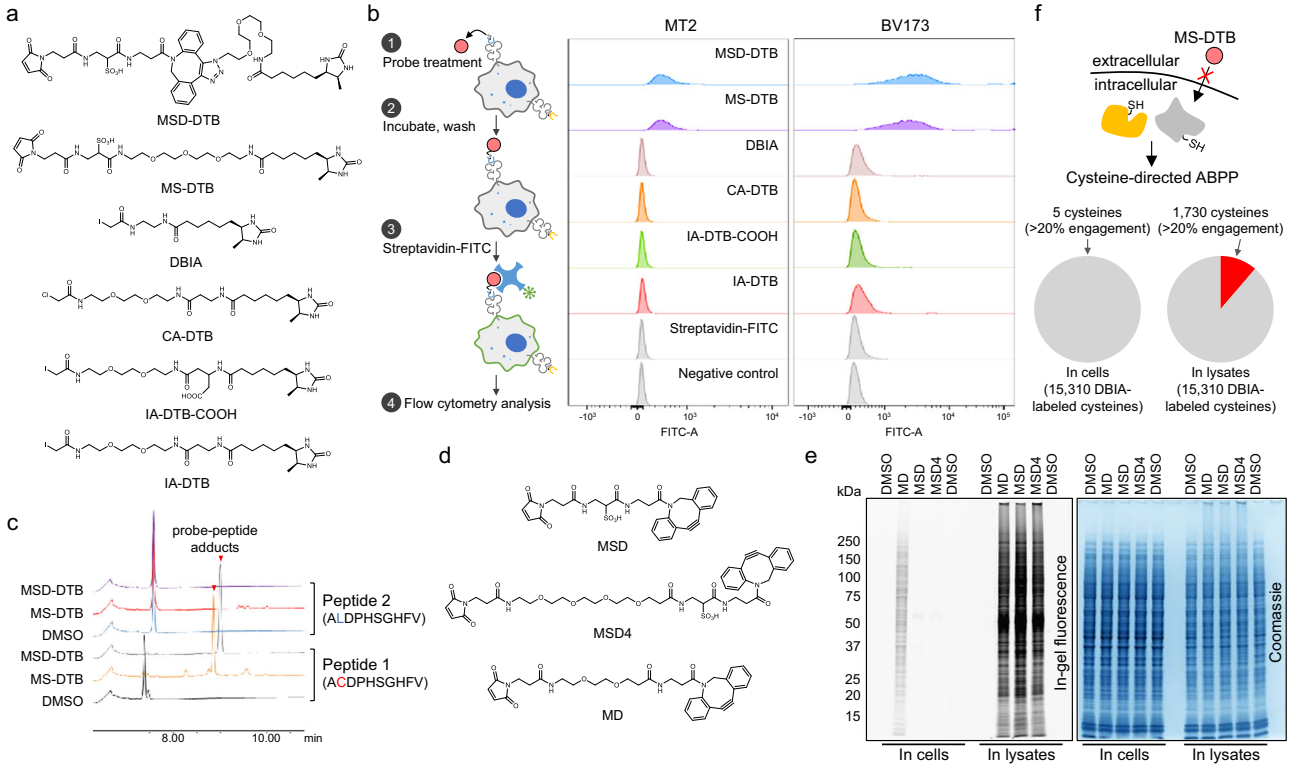

Fig. 1 | Development of cell-impermeable cysteine-reactive probes. a Structures of six reactivity probes. MSD-DTB, maleimide-sulfonate-dibenzocyclooctyne-DTB. MS-DTB, maleimide-sulfonate-DTB. DBIA, desthiobiotin iodoacetamide. IA-DTB, iodoacetamide-PEG-desthiobiotin. CA-DTB, chloroacetamide-PEG-desthiobiotin. IA-DTB-COOH, iodoacetamide-carboxylate-PEG-desthiobiotin. **b** MSD-DTB and MS-DTB probes exhibited greater cell surface labeling compared to the others in BV173 and MT2 cells. The result is a representative of three experiments ($n = 3$ independent replicates). Fluorescein isothiocyanate (FITC)-A represents the fluorescence intensity of FITC. **c**. LC-MS analyses revealed that MSD-DTB and MS-DTB probes modify cysteine, but not histidine, serine, and N-terminal amine. The result is a representative of two experiments ($n = 2$ independent replicates). **d** Structures of MD (maleimide-dibenzocyclooctyne), MSD (maleimide-sulfonate-dibenzocyclooctyne), and MSD4 (maleimide-sulfonate-dibenzocyclooctyne-PEG4). **e** In-gel fluorescence analyses revealed that sulfonated maleimide probes minimally labeled proteins in live cells, while yielding comparable levels of proteome labeling to its cell-permeable counterpart probe, MD, in cell lysates. The result is a representative of two experiments ($n = 2$ independent replicates). **f** Cysteine-directed activity-based protein profiling (ABPP) analyses revealed that MS-DTB modified five cysteines with >20% engagement out of 15,310 quantified cysteines in live cells, while it modified 1730 cysteines with >20% engagement in cell lysates. Data represent mean values ($n = 2$ independent replicates). Source data are provided as a Source Data file.

indicated minimal proteome labeling compared to a cell-permeable counterpart probe, maleimide dibenzocyclooctyne (MD), that lacks the sulfonate group (Fig. 1d, e). Conversely, treating cell lysates with these reactivity probes resulted in comparable levels of proteome labeling (Fig. 1e), suggesting that MSD and MSD4 probes are predominantly cell impermeable. Furthermore, we observed that the only uncharged maleimide probe, MD, exhibited cytotoxicity compared to the other sulfonated maleimide probes (Supplementary Fig. 2c). This underscores the cell impermeability of sulfonated maleimide probes incapable of accessing a wide range of intracellular proteins, potentially triggering stress and apoptosis[19]. Finally, we employed cysteine-directed ABPP to assess the global cysteine engagement of MS-DTB in cell lysates versus live cells. MS-DTB-treated samples were further labeled by DBIA for the quantification of DBIA-modified peptides. Reduced enrichment of DBIA-modified cysteine-containing peptides indicate the potential engagement of MS-DTB on these cysteines. The results revealed that among 15,310 quantified cysteines, 1730 cysteines showed >20% engagement by MS-DTB in cell lysates, whereas only 5 cysteines showed >20% engagement by MS-DTB in live cells (Fig. 1f and Supplementary Data 1). This suggests that MS-DTB has restricted access to intracellular proteins. Collectively, these findings indicate that sulfonated maleimide probes are predominantly cell impermeable.

Next, we sought to investigate the compatibility of sulfonated maleimide probes with proteomics workflow, specifically evaluating whether the probe-modified peptides can be effectively ionized and identified by orbitrap and ion trap mass analyzers. We incubated HEK293T cell lysates with MS-DTB and MSD-DTB probes, followed by trypsin digestion, enrichment with Streptavidin agarose beads, and subsequent analysis on a Tribrid mass spectrometer (Supplementary Fig. 2d). The results demonstrated the effective identification of cysteines modified by both sulfonated maleimide probes (Supplementary Fig. 2e and Supplementary Data 2), with MS-DTB probe exhibiting greater coverage than MSD-DTB probe (1833 versus 629 probe-modified cysteine-containing peptides). This difference is likely due to the smaller size of MS-DTB (molecular weight 690.8) compared to MSD-DTB (molecular weight 993.1), which may lead to enhanced ionization and better detection in the Orbitrap mass spectrometer. Therefore, for further proteomic studies aimed at identifying probe-modified cysteine-containing peptides, MS-DTB is likely the more suitable probe. Despite carrying a negatively charged sulfonate moiety, we observed a normal isotopic envelope profile of probe-modified peptides in positive mode on the orbitrap mass analyzer (Supplementary Fig. 2f). It is recognized that maleimide-modified cysteines can exist in both unhydrolyzed and hydrolyzed forms[20]. Our data revealed that approximately 20% of probe-modified peptides contain hydrolyzed maleimide (Supplementary Fig. 2e). Therefore, integrating both forms into the proteomics analysis pipeline would be a comprehensive approach.

Sulfonated maleimide probes label cysteines on MHC-I-bound antigens

We selected three cell lines – BV173, MT2 and MDA-MB-231 – to examine the potential of sulfonated maleimide probes in capturing cysteine-containing MHC-I bound antigens. These cell lines harbor commonly occurring *HLA* alleles (BV173: *HLA-A**02:01,30:01; MDA-MB-231: *HLA-A**02:01,02:17; and MT2: *HLA-A**24:02)[21,22]. Additionally, according to the TRON Cell Line Portal and Cancer Cell Line Encyclopedia, BV173 and MDA-MB-231 cells exhibit high expression levels of *HLA* genes and MHC-I proteins[22,23]. Our proteomics and flow cytometry studies indicated that MT2 cells also exhibited high MHC-I expression levels (see below). Thus, these cell lines serve as ideal models for studying potentially abundant cysteines within the MHC-I-associated immunopeptidome. To create control cell lines, we used Clustered Regularly Interspaced Short Palindromic Repeats (CRISPR)-Cas9 to knockout all six endogenous *HLA-A*, *HLA-B*, and *HLA-C* genes in these cell lines (referred to as *HLA* knockout hereafter). The knockout of *HLA* genes and the disruption of MHC-I proteins were confirmed through quantitative global proteomics and flow cytometry analysis (Fig. 2a, Supplementary Fig. 3a–d, Supplementary Fig. 4a and Supplementary Data 3).

We employed two approaches to assess sulfonated maleimide probes interacting with cysteines on MHC-I-bound antigens. In the first approach, we compared cell surface labeling by the probe in wildtype versus *HLA* knockout cells via flow cytometry. The results revealed a decrease in cell surface labeling by both MSD-DTB and MS-DTB probes in *HLA* knockout cells compared to wildtype cells across all three cell lines (Fig. 2b, Supplementary Fig. 3e, and Supplementary Fig. 4b), suggesting that the reduced cell surface labeling is likely attributable to MHC-I-bound antigens. We noticed a partial *HLA* knockout in MT2 cells, as indicated by global proteomics and flow cytometry analyses (Fig. 2a). We then sorted the MHC-I negative population in *HLA* partial knockout cells to generate *HLA* complete knockout cells (Fig. 2c, Supplementary Fig. 3f, Supplementary Fig. 4c, and Supplementary Data 3). Subsequently, we observed approximately a 50% decrease in cell surface labeling by MS-DTB in *HLA* complete knockout cells, compared to a 20% decrease in *HLA* partial knockout cells (Fig. 2d and Supplementary Fig. 4d). Furthermore, we measured cell surface labeling by a sulfonated lysine-reactive probe, N-hydroxysuccinimide (NHS)-sulfonate-biotin, and observed similar cell surface labeling in BV173 wildtype and *HLA* knockout cells (Fig. 2e and Supplementary Fig. 4e). Given that the majority of lysine residues in the extracellular milieu are from proteins, the cell surface labeling by the lysine-reactive probe is likely predominantly attributed to protein lysine residues and minimally affected by *HLA* knockout.

In the second approach, we employed an enzyme-linked immunosorbent assay (ELISA) to quantify probe-modified antigens within the pMHC-I complex. Given our demonstration that sulfonated maleimide probes do not penetrate cells and both MHC-I and β2-microglobulin lack unmodified cysteines in their extracellular domains, the presence of desthiobiotin in the pMHC-I complex implies the probe-modified peptide antigens (Fig. 2f). We treated MT2 and BV173 wildtype and *HLA* knockout cells with the MS-DTB probe, lysed the cells, enriched MHC-I protein using a pan-MHC antibody conjugated on the plate, and detected the abundance of desthiobiotin using Streptavidin-horseradish peroxidase (HRP). The results revealed the presence of MS-DTB in the pMHC-I complex in wildtype cells, with significantly lower levels observed in *HLA* knockout cells (Fig. 2f). Moreover, MS-DTB treatment did not affect pMHC-I folding, as indicated by the ELISA assay measuring the interaction between MHC-I and β2-microglobulin (Fig. 2g). Collectively, the findings from both approaches suggest that sulfonated maleimide probes modify cysteines on MHC-I-bound antigens.

With these assays, we explored the use of the MS-DTB probe to monitor shifts in cysteine reactivity of MHC-I-bound antigens in response to changes in pH and oxidative stress. Through ELISA assays, we assessed MS-DTB probe labeling on pMHC-I at pH of 5, 6, 7, and 8. The results showed that at pH 5, probe labeling on pMHC-I was significantly reduced, while labeling remained consistent at pH 6 and 7 (Supplementary Fig. 3g). At pH 8, however, probe labeling decreased dramatically, likely due to the dissociation of antigen peptides from the pMHC-I complex at this pH, as previously reported[24]. These findings suggest that pH changes can influence cysteine reactivity on MHC-I-bound antigens. Additionally, we investigated the impact of oxidative stress by pretreating cells with varying concentrations of hydrogen peroxide, which is known to induce cysteine oxidation[25] and, consequently, may block the reactive cysteines on MHC-I bound peptides. ELISA assays revealed decreased probe labeling on the pMHC-I complex under this condition (Supplementary Fig. 3h), indicating that the

https://doi.org/10.1038/s41467-024-54139-8

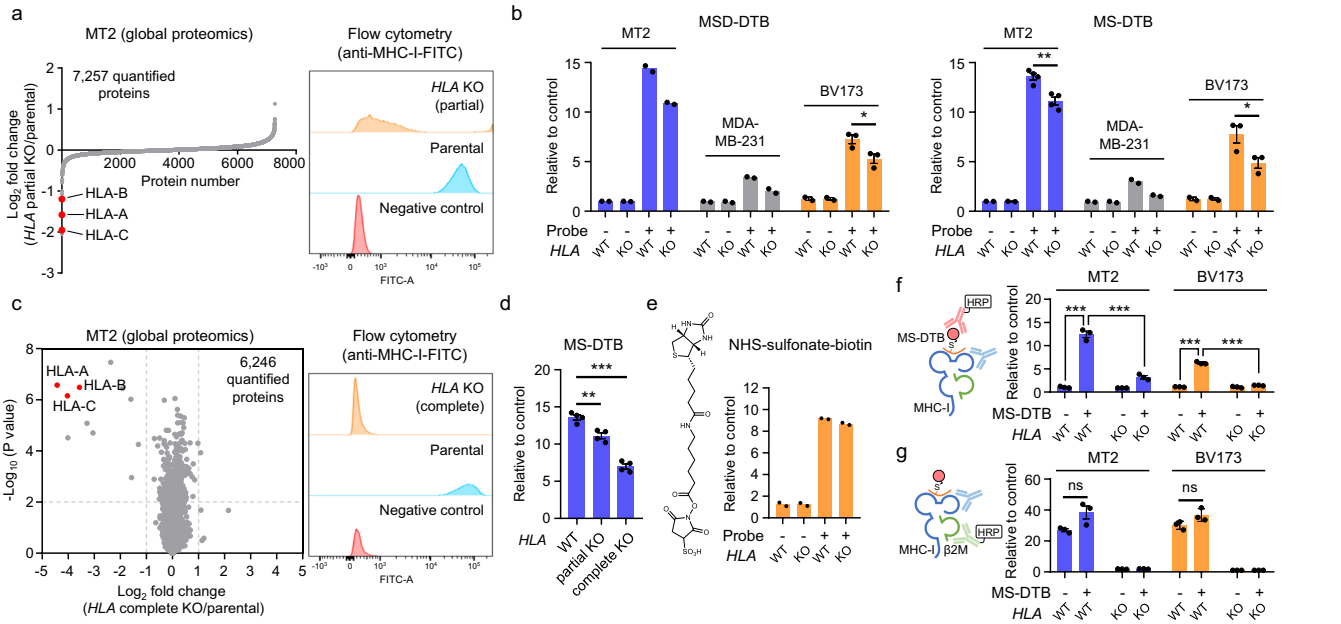

Fig. 2 | Sulfonated maleimide probes modify cysteines on MHC-I-bound antigens. a Quantitative global proteomics and flow cytometry studies confirmed the knockout (KO) of *HLA* class I genes in MT2 cells. Global proteomics data represent mean values (n = 3 independent replicates). The result of flow cytometry analysis is a representative of two experiments (n = 2 independent replicates). **b** Flow cytometry analyses measuring Streptavidin-FITC staining on *HLA* wildtype (WT) and KO cells treated with the MSD-DTB or MS-DTB probe. Data represent mean values (n = 2 independent replicates in MT2 and MDA-MB-231 cells treated with MSD-DTB, and MDA-MB-231 cells treated with MS-DTB) and mean values ± SEM (n = 3 independent replicates in BV173 cells treated with MSD-DTB and MS-DTB, and n = 4 independent replicates in MT2 cells treated with MS-DTB). The statistical significance was assessed using unpaired two-tailed Student's t-tests. P values were 0.037, 0.0029, and 0.048. **c** Quantitative global proteomics and flow cytometry studies confirmed the complete knockout of *HLA* class I genes in MT2 cells. Global proteomics data represent mean values (n = 3 independent replicates). P values were calculated by two-sided t test and adjusted using Benjamini-Hochberg correction for multiple comparisons. The result of flow cytometry analysis is a representative of two experiments (n = 2 independent replicates). **d** Flow cytometry analyses measuring Streptavidin-FITC staining on MT2 parental and *HLA* knockout cells treated with MS-DTB. Data represent mean values ± SEM (n = 4 independent replicates). The statistical significance was assessed using unpaired two-tailed Student's t-tests. P values were 0.0029 and 9.2×10^{-6}. **e** Structure of NHS-sulfonate-biotin and flow cytometry analyses measuring Streptavidin-FITC staining on BV173 *HLA* wildtype and knockout cells treated with NHS-sulfonate-biotin. Data represent mean values (n = 2 independent replicates). NHS, N-hydroxysuccinimide. **f** ELISA assay measuring MS-DTB in the pMHC-I complex. Data represent mean values ± SEM (n = 3 independent replicates). The statistical significance was assessed using unpaired two-tailed Student's t-tests. P values were 8.1×10^{-5}, 0.00028, 6.2×10^{-6}, and 8.7×10^{-6}. HRP, horseradish peroxidase. **g** ELISA assay measuring MHC-I and β2-microglobulin (β2M) assembly. Data represent mean values ± SEM (n = 3 independent replicates). The statistical significance was assessed using unpaired two-tailed Student's t-tests. Source data are provided as a Source Data file.

MS-DTB probe effectively detects alterations in cysteine reactivity due to changes in the oxidative environment.

MHC-I immunopeptidome exhibits distinct cysteine reactivities

Next, we employed immunopeptidomics to examine the abundance and positioning of probe modified cysteines within the MHC-I immunopeptidome. MT2 and BV173 cells were treated with MS-DTB, then washed twice with phosphate buffered saline (PBS) before harvesting to remove free probes from the culture media. This was followed by cell lysis and immunoprecipitation using a pan-MHC-I antibody to enrich the pMHC-I complex. The immunopeptidome was eluted and analyzed using MS (Fig. 3a). During the data search, we included two dynamic modifications on cysteines: 1) MS-DTB (both unhydrolyzed and hydrolyzed forms); and 2) cysteinylation, a frequently observed cysteine modification in immunopeptidomics studies[26]. We identified 3,311 and 2,080 8-13-mer peptides in MT2 and BV173 cells, respectively (Fig. 3b and Supplementary Data 4). Parallel immunopeptidomics conducted in *HLA* knockout cells resulted in no 8-13-mer peptides identified in either cell line (Supplementary Data 4). To validate the absence of identified peptides in *HLA* knockout cells, we analyzed the MS1 base peak chromatograms of immunopeptidomics data from *HLA* wildtype and knockout cells. As shown in Supplementary Fig. 5a, *HLA* wildtype cells exhibit a normal MS1 trace pattern with dispersed and individual peaks, whereas *HLA* knockout cells show only a few remaining peaks. The MS1 spectra of these peaks reveal singly charged nonpeptide products (Supplementary Fig. 5b). We did not find evidence of multiply charged peptide products in these peaks in *HLA* knockout cells. This low peptide background in *HLA* knockout cells is likely attributed to the effective *HLA* knockout and the use of a specific anti-MHC-I antibody (clone W6/32) in immunopeptidomics, which generates minimal background signal.

Motif analysis of 9-mer peptides, the most preferred length for MHC-I[27] (Supplementary Fig. 5c), revealed a close alignment with reported distribution patterns associated with the corresponding *HLA* alleles (Fig. 3c and Supplementary Fig. 5d)[28], indicating effective enrichment of the MHC-I immunopeptidome. Similar matched distribution patterns were also observed for 8-mer and 10-mer MHC-I bound peptides (Supplementary Fig. 5d). Among all the identified antigens, 282 and 216 contain cysteine residues in MT2 and BV173 cells, respectively (Fig. 3b). Motif analysis of cysteine-containing 9-mer antigens revealed a similar pattern to that of all 9-mer antigens (Fig. 3c), indicating the confident identification of these cysteine-containing peptides binding to MHC-I. The analysis of cysteinylation on MHC-I-bound antigens revealed enrichment primarily at positions 7 and 8 (Fig. 3d), consistent with the distribution motif reported in a recent study[26]. We then conducted immunopeptidomics on untreated MT2 and BV173 cells and identified 3,449 and 2,232 8-13-mer peptides, respectively (Supplementary Fig. 5e and Supplementary Data 4). Among these, 236 peptides in MT2 cells and 160 peptides in BV173 cells contained cysteine residues, constituting 6.8% and 7.2% of the total

https://doi.org/10.1038/s41467-024-54139-8

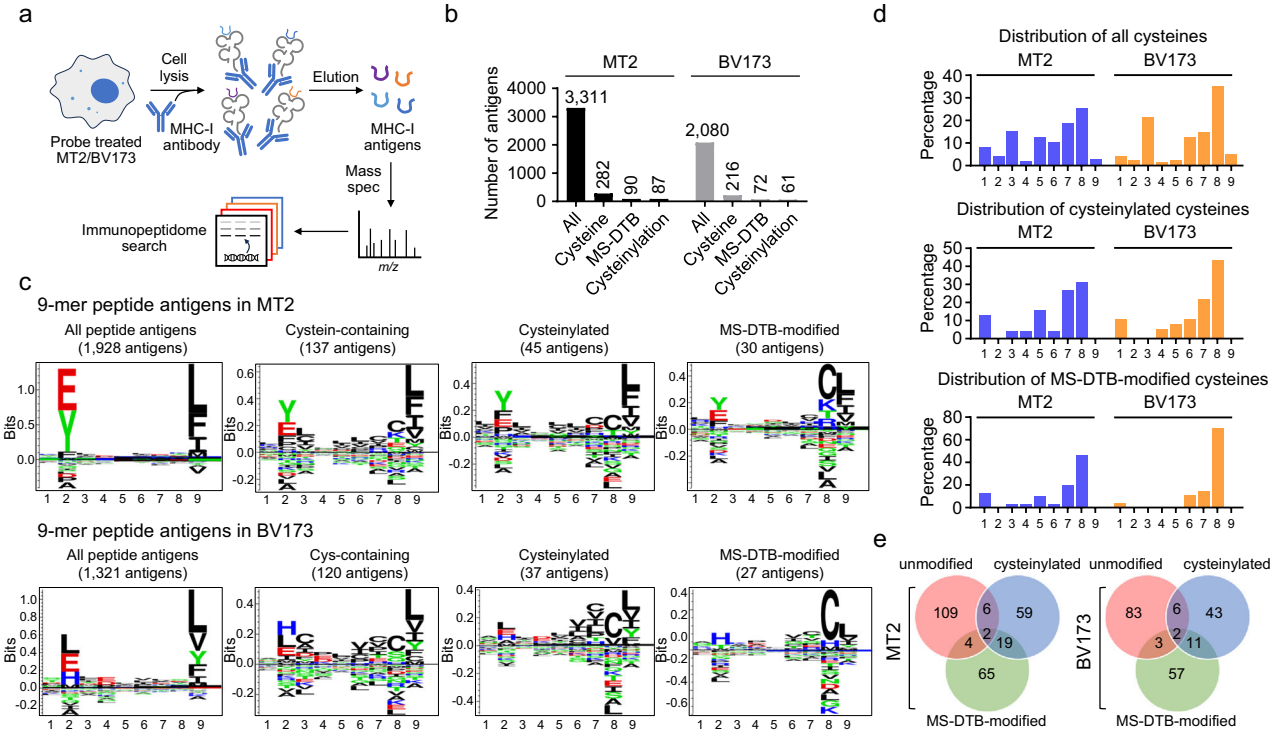

Fig. 3 | MHC-I immunopeptidome exhibits distinct cysteine reactivities. **a** Schematic representation of the immunopeptidomics workflow. **b** The number of 8-13-mer MHC-I-associated peptides in MT2 and BV173 cells treated with 50 μM of MS-DTB. The result is a representative of two experiments ($n = 2$ independent replicates). **c** Motif analysis of all 9-mer MHC-I-bound antigens, cysteine-containing 9-mer MHC-I-bound antigens, cysteinylated 9-mer MHC-I-bound antigens, and MS-DTB-modified 9-mer MHC-I-bound antigens. **d** Distribution of all cysteines, cysteinylated cysteines, and MS-DTB-modified cysteines on 9-mer peptide antigens in MT2 and BV173 cells. **e** Venn diagram of MHC-I-bound antigens with unmodified, cysteinylated, and MS-DTB-modified cysteines. Source data are provided as a Source Data file.

identified peptides in each cell line, respectively (Supplementary Fig. 5f). In comparison, MS-DTB-treated cells exhibited slightly higher numbers and percentages of cysteine-containing peptides (8.5% and 10.4% in MT2 and BV173 cells, respectively).

Approximately 30% of the identified cysteines in both cell lines were found to be modified by MS-DTB. Notably, there was minimal overlap between MS-DTB-modified and unmodified cysteine-containing antigens (Fig. 3e and Supplementary Fig. 5g). We surmise that a portion of cysteine-containing antigens may harbor unreactive cysteines that are inaccessible to even high concentration (50 μM) of maleimide probes. Conversely, the cysteines modified by MS-DTB may exist in a solvent-exposed reactive state, making them effectively trackable by maleimide probes, leading to complete labeling and the observed pattern of minimal overlap between unmodified and probe-modified antigen cysteines. Among all the MS-DTB-modified cysteines on 9-mer antigens, there is a preference for MS-DTB labeling at position 8 in both MT2 and BV173 cells (Fig. 3d). We then analyzed 8-mer MS-DTB-modified peptides and observed that the MS-DTB probe preferentially labeled cysteines at position 7 on 8-mer antigens (Supplementary Fig. 5h). These patterns indicate that the MS-DTB probe may preferentially label the second-to-last position of MHC-I-bound antigens. For 10-mer antigens, the number of MS-DTB-labeled peptides is relatively small (five each in MT2 and BV173), which may limit the statistical representativeness of the distribution pattern. Moreover, the analysis of cysteine-containing longer antigens revealed that the majority were modified by MS-DTB (Supplementary Fig. 5i). We speculate that these longer cysteine-containing antigens may have increased cysteine solvent accessibility, which could lead to enhanced probe labeling.

Next, we conducted overlap analyses comparing unmodified cysteines in untreated samples with MS-DTB-modified cysteines in treated samples for both MT2 and BV173 cells. A small subset of unmodified cysteines in the untreated samples were labeled by the MS-DTB probe (Supplementary Fig. 5j), indicating their highly reactive state that can be detected by the probe. In contrast, the overlap analysis of unmodified cysteines in both untreated and treated samples revealed a substantially increased overlap (Supplementary Fig. 5j), suggesting a population of unreactive cysteines that are inaccessible to the MS-DTB probe. Notably, many MS-DTB-modified cysteines were not identified in the untreated samples in their unmodified state. We speculate that these cysteine-containing peptides might be unstable or undergo oxidation during sample preparation, making them difficult to identify. However, MS-DTB probe treatment may stabilize these peptides and/or prevent potential oxidation, thereby enabling their identification.

BV173 cells have well-characterized *HLA* class I alleles, including *HLA-A**02:01, *HLA-A**30:01, *HLA-B**15:10, *HLA-B**18:01, *HLA-C**03:04, and *HLA-C**12:03[22]. By comparing the 9-mer antigen distribution motifs associated with these *HLA* alleles in the MHC Motif Atlas to those in our immunopeptidomics data, we observed abundant expression of MHC-I proteins encoded by *HLA-A**02:01, *HLA-B**15:10, and *HLA-B**18:01 (Supplementary Fig. 6a, b). We did not observe clear distribution motifs for the remaining three alleles, suggesting their low abundance under our experimental conditions. In our immunopeptidomics study, although we used a pan-MHC-I antibody to enrich all pMHC-I complexes, the differential amino acids at position 2 allowed us to group the identified antigens according to their presumed *HLA* allele associations. This analysis revealed distinct distribution motifs of MS-DTB-modified 9-mer antigens associated with *HLA-A**02:01, *HLA-B**15:10, and *HLA-B**18:01 (Supplementary Fig. 6c). Notably, the majority of MS-DTB-modified peptides were associated with *HLA-B**15:10. Additionally, MS-DTB exclusively labeled the second-to-last position in

https://doi.org/10.1038/s41467-024-54139-8

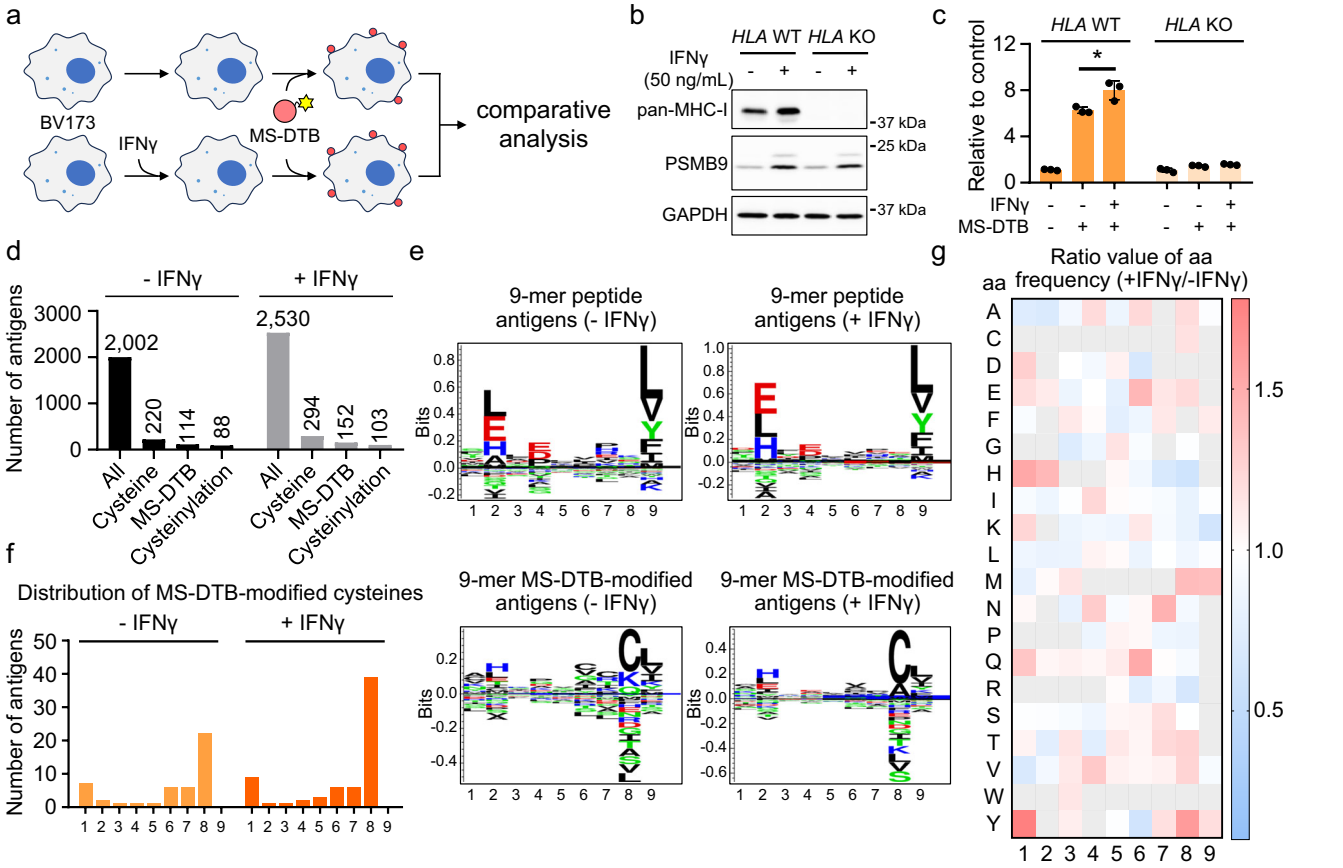

Fig. 4 | Using sulfonated maleimide probes to assess changes in cysteine reactivity of MHC-I bound antigens upon IFNγ stimulation. a Schematic representation of comparative analysis in interferon gamma (IFNγ)-stimulated versus non-stimulated BV173 cells. **b** Western blot analysis of MHC-I and PSMB9 expression in BV173 cells stimulated with IFNγ (50 ng/mL, 24 h). The result is a representative of two experiments ($n = 2$ independent replicates). **c** ELISA assay measuring the presence of MS-DTB in the pMHC-I complex with or without IFNγ stimulation in BV173 cells. Data represent mean values ± SEM ($n = 3$ independent replicates). The statistical significance was evaluated through unpaired two-tailed Student's *t*-tests. *P* value was 0.025. **d** The number of 8-13-mer MHC-I-associated peptides in IFNγ-stimulated versus non-stimulated cells. **e**. Motif analysis of all 9-mer MHC-I-bound antigens and MS-DTB-modified MHC-I-bound antigens. **f** Distribution of MS-DTB-modified cysteines on 9-mer MHC-I-bound antigens in IFNγ-stimulated versus non-stimulated cells. **g** Heatmap showing the ratio values of amino acid (aa) frequency in IFNγ-stimulated versus non-stimulated cells. The percentage of each aa relative to all amino acids at each position was calculated to derive the ratio values between IFNγ-stimulated and non-stimulated cells. A gray shade indicates aa with a percentage below 2%. Source data are provided as a Source Data file.

peptides bound to MHC-I encoded by *HLA-B**15:10. These allele-driven differences may stem from variations in groove depth, which present an intriguing avenue for further investigation.

MT2 cells, on the other hand, do not have well-determined *HLA* class I alleles listed in public databases, but literature reports indicate they carry *HLA-A**24:02 and *HLA-B**40:01[29]. The distribution motif of 9-mer antigens associated with these two alleles in the MHC Motif Atlas aligns with the observations from our immunopeptidomics study (Supplementary Fig. 6a, b). Our data did not reveal additional peptides associated with *HLA* alleles beyond *HLA-A**24:02 and *HLA-B**40:01. Therefore, it is likely that MT2 predominantly expresses MHC-I proteins encoded by *HLA-A**24:02 and *HLA-B**40:01. Analysis of the immunopeptidomics data revealed that the MS-DTB probe labels peptides associated with *HLA-A**24:02 and *HLA-B**40:01 with similar efficacy (Supplementary Fig. 6d). The distribution patterns of probe-modified cysteines are largely consistent between both alleles, with preferential labeling at the second-to-last position in each case. However, the MS-DTB probe labels cysteine at position 1 in peptides bound to *HLA-A**24:02 but not *HLA-B**40:01. One explanation may be differences in groove conformation that result in a less reactive state for cysteines at position 1 in peptides associated with *HLA-B**40:01. We also speculate that the negatively charged glutamate at position 2 in peptides associated with *HLA-B**40:01 may repel the negatively charged MS-DTB probe, preventing interaction with adjacent residues.

Recent studies reveal that post-translational modifications (PTMs) can occur on MHC-I-bound antigens[26]. To investigate this, we examined various abundant PTMs reported on pMHC-I[26], including lysine acetylation, lysine dimethylation, arginine dimethylation, asparagine deamidation, serine phosphorylation, and threonine phosphorylation, in our immunopeptidomics studies. Only a few of these PTMs co-occurred with antigens modified by MS-DTB (Supplementary Data 4). This limited number of co-modified peptides may not provide sufficient statistical power to determine how PTMs influence MS-DTB modification. Nonetheless, exploring how PTMs affect cysteine reactivity within the immunopeptidome presents a valuable area for further investigation.

Assessment of reactive cysteine alternations in the immunopeptidome

MHC-I antigen presentation undergoes regulation through various mechanisms occurring during both transcriptional and post-translational stages[30]. For example, immunoproteasome expression can influence the antigens presented by MHC-I[31]. To explore potential alterations in reactive cysteines on MHC-I-bound antigens, we treated

https://doi.org/10.1038/s41467-024-54139-8

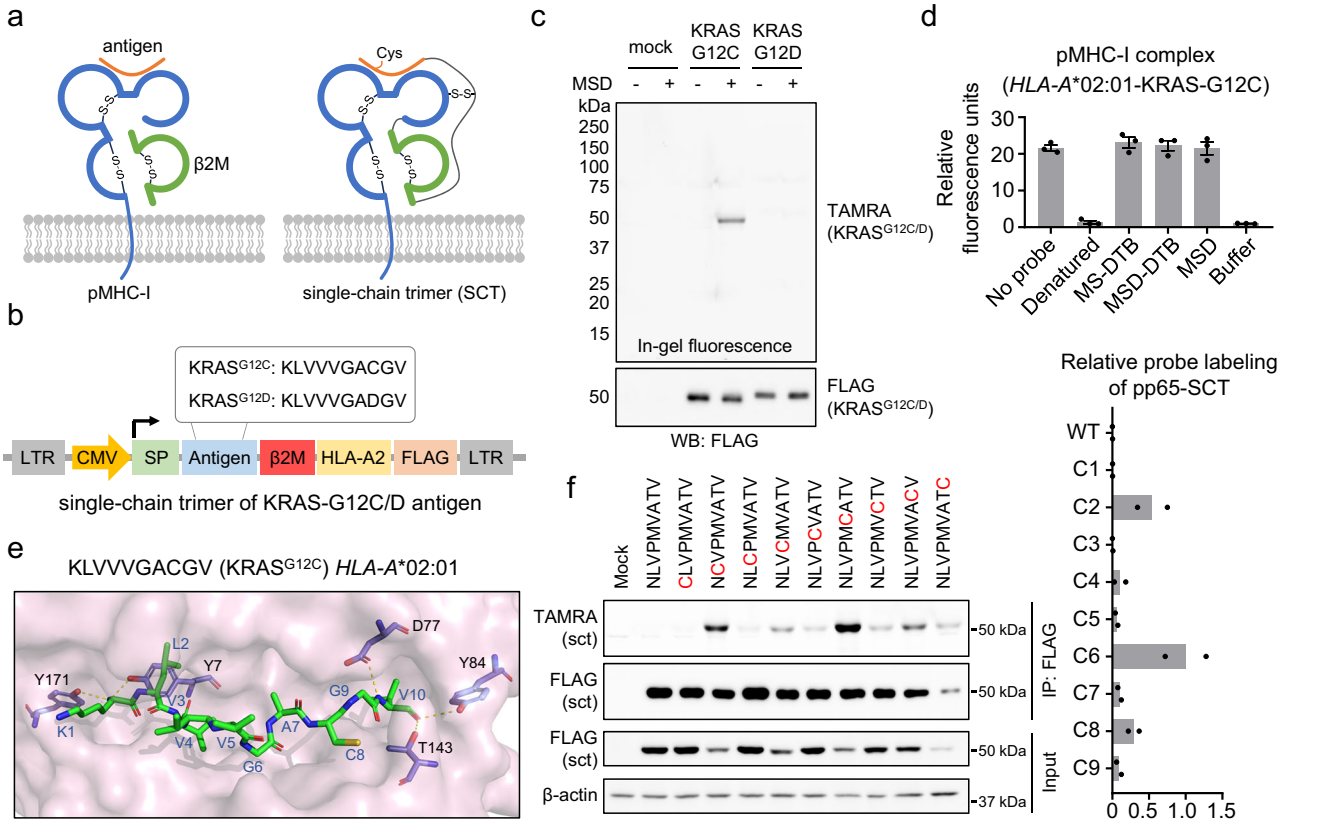

Fig. 5 | Mapping reactive cysteines on MHC-I-bound antigens using the single-chain trimer model. a Schematic representation of a native pMHC-I complex and a single-chain trimer. **b** Constructs of SCTs of *HLA-A**02:01 presenting the KRAS-G12C and KRAS-G12D neoantigens. SCT, single-chain trimer. LTR, long-terminal repeats. CMV, cytomegalovirus. SP, signal peptide. **c** In-gel fluorescence analysis of KRAS-G12C-SCT and KRAS-G12D-SCT from HEK293T cells treated with the MSD probe (50 μM, 30 min). The result is a representative of three experiments ($n = 3$ independent replicates) TAMRA, tetramethylrhodamine. **d** ELISA assay measuring the assembly of MHC-I and β2-microglobulin in the presence of sulfonated maleimide probes. Data represent mean values ± SEM ($n = 3$ independent replicates). **e** Modeling studies suggest that the cysteine in the KRAS-G12C neoantigen is exposed to the solvent when bound to MHC-I. **f** In-gel fluorescence analysis of SCTs of *HLA-A**02:01 presenting pp65 antigens with cysteines introduced at positions 1–9 from HEK293T cells treated with the MSD probe (50 μM, 30 min). The bar graph represents quantification of the TAMRA/FLAG ratio values following FLAG immunoprecipitation (IP). Data represent mean values ($n = 2$ independent replicates). Source data are provided as a Source Data file.

BV173 cells with interferon-gamma (IFNγ), a cytokine known to stimulate immunoproteasome expression (Fig. 4a). We confirmed IFNγ-induced immunoproteasome expression by observing increased levels of PSMB9, a subunit of the immunoproteasome (Fig. 4b)[31]. We also noted a moderate increase in MHC-I expression, consistent with previous findings[32]. Subsequently, using ELISA assays, we observed significantly enhanced MS-DTB engagement within the pMHC-I complex in *HLA* wildtype, but not knockout cells (Fig. 4c). This increased engagement could result from increased cysteine reactivity or abundance.

Further investigation via immunopeptidomics revealed 2530 8-13-mer MHC-I-bound peptides in IFNγ-stimulated cells versus 2002 in non-stimulated cells (Fig. 4d and Supplementary Data 5), indicating an overall enhancement of MHC-I presented antigens with IFNγ stimulation. Consequently, the number of MS-DTB-modified 8-13-mer peptides also increased upon IFNγ simulation (Fig. 4d). Motif analysis of 9-mer MHC-I-bound peptides comparing IFNγ-stimulated versus non-stimulated cells showed a consistent pattern (Fig. 4e), suggesting that IFNγ stimulation does not alter the overall pattern of MHC-I presented antigens. Interestingly, IFNγ stimulation primarily increased MS-DTB labeling at position 8 of 9-mer MHC-I-bound peptides, with other modified positions remaining unaffected (Fig. 4f, g). Collectively, these findings demonstrate the use of sulfonated maleimide probes in mapping changes in reactive cysteines on MHC-I-associated peptide antigens during altered physiological processes.

Mapping reactive cysteines using the single-chain trimer

Single-chain trimers (SCTs) are engineered constructs comprising covalently linked single chains of MHC-I, β2-microglobulin, and displayed antigenic peptides (Fig. 5a)[33]. SCTs retain structural integrity similar to native pMHC-I complexes and can activate T cells[34,35], making them valuable models for investigating MHC-I antigen presentation and function. In our study, employing SCTs enables the precise generation of constructs encoding pMHC-I that present specific cysteine-containing antigens. To this end, we created two SCTs of *HLA-A**02:01 presenting previously reported KRAS neoantigens: one containing the G12C mutation (KLVVVGACGV)[10,11] and the other containing the G12D mutation (KLVVVGADGV)[36] (Fig. 5b). Both SCTs were incorporated with a C-terminal intracellular FLAG tag. HEK293T cells were transfected with KRAS-G12C- or KRAS-G12D-SCT and treated with the MSD probe. After cell lysis, SCTs were enriched via FLAG immunoprecipitation, followed by an azide-alkyne cycloaddition[17,18] with TAMRA azide, enabling visualization of MSD-modified SCTs via in-gel fluorescence. The results revealed that KRAS-G12C-SCT was labeled by the MSD probe, whereas KRAS-G12D-SCT showed no detectable labeling (Fig. 5c). Since there are no extracellular unmodified cysteines on MHC-I, β2-microglobulin, and linker components in the SCT constructs (Supplementary Fig. 7), the labeling signal is likely attributed to the cysteine in the KRAS-G12C neoantigen. Furthermore, we conducted an ELISA assay by incubating sulfonated maleimide probes with recombinant pMHC-I (*HLA-A**02:01) bound to the KRAS-G12C

https://doi.org/10.1038/s41467-024-54139-8

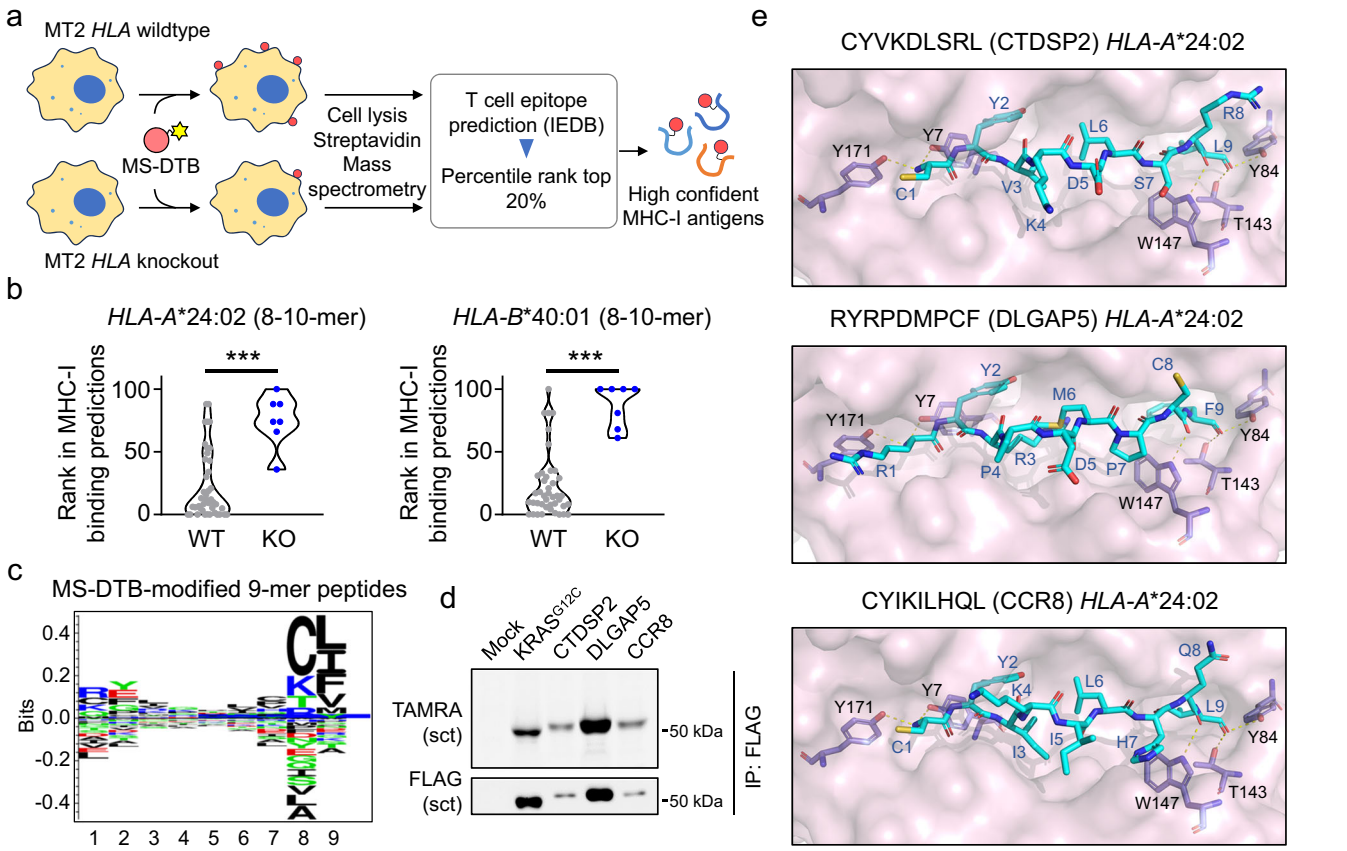

Fig. 6 | Reactivity-based antigen profiling for the discovery of reactive cysteines on MHC-I-bound antigens. a Schematic representation of the reactivity-based antigen profiling workflow. **b** Violin plot comparing the predicted MHC-I binding ranks of MS-DTB-enriched 8–10-mer peptides in MT2 parental and *HLA* knockout cells. The statistical significance was evaluated through unpaired two-tailed Student's *t*-tests. *P* values were 1.2×10^{-5} and 6.2×10^{-8}. The result is a representative of two experiments ($n = 2$ independent replicates). **c** Motif analysis of MS-DTB-modified 9-mer peptides identified in MT2 parental cells. The result is a representative of two experiments ($n = 2$ independent replicates). **d** Validation of MS-DTB-modified peptides using SCTs. The result is a representative of two experiments ($n = 2$ independent replicates). **e**. Modeling studies indicate that cysteines in the MS-DTB-modified peptides are solvent-exposed when forming pMHC-I complexes. Source data are provided as a Source Data file.

neoantigen (KLVVVGACGV). The data indicate that probe incubation did not disrupt the proper folding of the pMHC-I complex (Fig. 5d). Modeling studies using *HLA-A**02:01 revealed that Y7 and Y171 on MHC-I formed hydrogen bonds with the N-terminal NH of KRAS-G12C neoantigen. On the other end, D77, Y84 and T143 in the F-pocket of MHC-I formed hydrogen bonds with the C-terminal valine (Fig. 5e). The overall confirmation of the KRAS-G12C neoantigen exposures cysteine at position 8 to the solvent, resulting in its reactive state.

Subsequently, we selected a non-cysteine 9-mer antigen (NLVPMVATV), known as pp65 viral antigen, derived from cytomegalovirus and presented by MHC-I encoded by *HLA-A**02:01[37]. We employed the SCT model to explore the reactivity of cysteines individually introduced at all positions of the pp65 antigen (pp65-C1-C9, Fig. 5f). The results revealed relatively low expressions of SCTs when cysteines were introduced at the anchoring positions 2 and 9, indicating that the presence of cysteines at these sites may disrupt the proper folding of the complex. Notably, MSD labeling patterns exhibited variations among these cysteine-containing antigens (Fig. 5f). For instance, pp65-C2 showed strong probe labeling despite low expression levels. In contrast, pp65-C3 showed minimal labeling despite having the highest expression levels. These findings indicate that cysteines on MHC-I-bound antigens may exhibit distinct reactivities, and the sulfonated maleimide probes are capable of mapping these variations using the SCT model. Interestingly, the highest labeling observed at pp65-C6 differs from the pattern observed in the immunopeptidomics studies, which indicate the highest probe labeling at positions adjacent to the anchoring residue (Fig. 3d and Supplementary Fig. 5h). This discrepancy may result from the statistical likelihood of a probe-labeled cysteine being adjacent to the anchor residue. However, individual antigens may not always adhere to this pattern and can present exceptions.

Reactivity-based profiling of cysteines in the immunopeptidome

Building on the principle of cysteine-directed ABPP[13,38], we explored whether sulfonated maleimide probes could facilitate global mapping of reactive cysteines on MHC-I-bound antigens. We developed a chemical proteomics strategy wherein cells are treated with the MS-DTB probe, followed by cell lysis, streptavidin enrichment, and MS analysis to identify reactive cysteines on MHC-I-bound antigens. To validate this platform, we initially overexpressed KRAS-G12C in BV173 parental and *HLA* knockout cells, then treated them with MS-DTB (Supplementary Fig. 8a). Subsequent proteomic analysis revealed the identification of MS-DTB-modified KRAS-G12C neoantigen only in BV173 parental cells, but not in *HLA* knockout cells (Supplementary Fig. 8b), indicating the feasibility of utilizing this approach to further profile reactive antigen cysteines in an untagged manner.

Next, we implemented this reactivity-based antigen profiling strategy in MT2 parental and *HLA* knockout cells, aiming to identify probe-modified reactive cysteine-containing MHC-I antigens (Fig. 6a). To evaluate the effectiveness of the probe in enriching MHC-I bound

https://doi.org/10.1038/s41467-024-54139-8

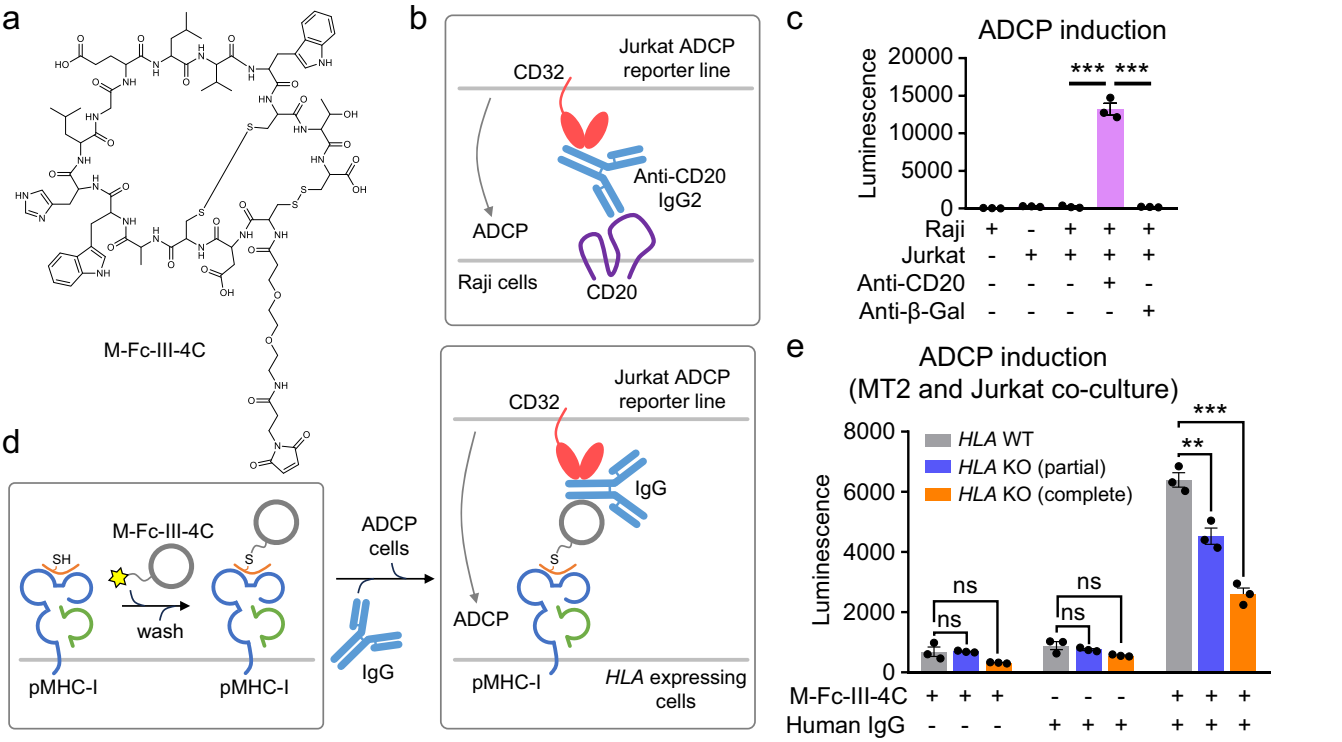

Fig. 7 | Targeting reactive cysteines on MHC-I-bound antigens to induce ADCP. **a** Structure of M-Fc-III-4C. **b** Schematic representation of anti-CD20-induced antibody-dependent cellular phagocytosis (ADCP) between Jurkat ADCP reporter cells and Raji cells. IgG, immunoglobulin G. **c** ADCP assay measuring luciferase activation in Jurkat-Luc NFAT-CD32 cells after co-culturing with Raji cells in the presence of anti-CD20 antibody. Anti-β-galactosidase (Gal) antibody served as a negative control. Data represent mean values ± SEM (n = 3 independent replicates). The statistical significance was evaluated through unpaired two-tailed Student's t-tests. P values were 0.000078 and 0.000075. **d** Schematic representation of targeting reactive cysteines on MHC-I-bound antigens to induce ADCP. **e** ADCP assay measuring luciferase activation in Jurkat-Luc NFAT-CD32 cells after co-culturing with M-Fc-III-4C-treated MT2 parental and *HLA* knockout cells in the presence of human IgG. Data represent mean values ± SEM (n = 3 independent replicates). The statistical significance was evaluated through unpaired two-tailed Student's t-tests. P values were 0.0066 and 0.00027. Source data are provided as a Source Data file.

peptides, we compared the MHC-I binding ranks predicted by IEDB for all probe-enriched 8-10-mer antigens in MT2 parental and *HLA* knockout cells. The results indicated that probe-enriched peptides had significantly higher ranks for both *HLA-A**24:02 and *HLA-B**40:01 in *HLA* wildtype cells compared to *HLA* knockout cells, suggesting that the MS-DTB probe is effective at enriching peptides bound to MHC-I (Fig. 6b). Nonetheless, the MS-DTB probe can still enrich peptides originating from other sources. To mitigate this effect, we incorporated three filters into the workflow: 1) restriction to 8-12-mer peptides in the search engine to exclude longer peptides from the pMHC-II complex; 2) utilization of a T cell epitope prediction algorithm to retain only top-ranked peptides for *HLA-A**24:02 or *HLA-B**40:01; and 3) selection of probe-modified peptides identified exclusively in MT2 parental cells, excluding peptides identified in *HLA* knockout cells. Using these filters, 95 MS-DTB-modified 8-12-mer peptides were identified in MT2 parental cells, with 39 falling within the top 20% ranking range using the T cell epitope prediction algorithm in IEDB (Supplementary Fig. 8c and Supplementary Data 6). Motif analysis of 9-mer MS-DTB-modified peptides revealed a distribution pattern associated with the *HLA* alleles (*HLA-A**24:01 and *HLA-B**40:01) in MT2 cells (Fig. 6c). Notably, the preferred MS-DTB labeling site at position 8 is consistent with findings from immunopeptidomics (Fig. 3c, d). Conversely, in MT2 *HLA* knockout cells, among 43 MS-DTB-modified 8-12-mer peptides, only 3 are within the top 20% ranking range (Supplementary Fig. 8c). Analysis of allele-specific MS-DTB modification of cysteines revealed distribution patterns similar to those observed in the immunopeptidomics study (Supplementary Fig. 8d and Supplementary Fig. 6d), further confirming the reliability of our findings regarding allele-specific probe modifications of antigen cysteines.

Next, we compared probe-pulldown experiments, focusing on 8-10-mer MS-DTB-modified peptides ranked within the top 20% ranking range, with 8-10-mer MS-DTB-modified peptides identified in immunopeptidomics. Of the 29 probe-modified peptides in probe-pulldown experiments, 9 were identified in both methods (Supplementary Fig. 9a). We then compared the MHC-I binding ranks of these 9 peptides with the 20 probe-modified peptides identified solely through probe-pulldown experiments. The result reveals that the 9 peptides identified by both methods have significantly higher MHC-I (*HLA-A**24:02) binding ranks compared to the remaining 20 peptides (Supplementary Fig. 9b). We surmise that the relatively lower MHC-I (*HLA-A**24:02) binding affinity of these 20 peptides may lead to their partial loss during sample preparation in immunopeptidomics. Conversely, in probe-pulldown experiments, the covalent interaction between the MS-DTB probe and these antigens may circumvent this limitation, allowing for the identification of probe-modified peptides.

Since the MS-DTB probe may label MHC-II-associated peptides and cell surface proteins with unmodified cysteines, we then analyzed the mass spectrometry data to focus on 13-16-mer peptides[39] within the top 20% ranks according to the IEDB MHC-II epitope prediction algorithm. The number of 13-16-mer peptides potentially associated with MHC-II is similar between MT2 parental and *HLA* knockout cells, which have comparable MHC-II protein expression (Supplementary Fig. 3f, Supplementary Fig. 10 and Supplementary Data 6). Regarding cell surface proteins, we re-analyzed the ABPP results from in-cell MS-DTB treatment (Fig. 1f). Among the 39 cysteines showing ≥15% engagement

by the MS-DTB probe (Supplementary Data 1), only one cysteine, SORT_C86, is located in the extracellular domain of this transmembrane protein. Given the oxidizing extracellular environment, where most extracellular protein cysteines form disulfide bonds[12], this data suggests that, at least in the HEK293T cell line, MS-DTB labeling of cell surface proteins is minimal. We recognize that our analysis focused on engagements of ≥15%, as lower engagements (<15%) might be indistinguishable from experimental variation. Thus, extracellular cysteines with low stoichiometric engagement by the MS-DTB probe may have been overlooked.

Next, we employed SCTs of *HLA-A**24:02 to validate three MS-DTB-enriched antigens: CTDSP2 (CYVKDLSRL), DLGAP5 (RYRPDMPCF), and CCR8 (CYIKILHQL). In-gel fluorescence analysis demonstrated effective labeling of all three antigens by the MSD probe (Fig. 6d). Moreover, a modeling study using *HLA-A**24:02 revealed that the anchor residues at positions 2 and 9 of all three antigen peptides fit into the B- and F-pockets, respectively (Fig. 6e). In the case of DLGAP5, where cysteine resides at position 8, the phenylalanine at anchoring position 9 is buried within the F-pocket and forms hydrogen bonds with Y84 and T143 in MHC-I. The carbonyl group of C8 is fixed with the NH in W147 through a hydrogen bond, which causes the cysteine at position 8 to be solvent exposed. As for CTDSP2 and CCR8 antigens, where cysteine is situated at position 1, the hydroxyl groups of Y7 and Y171 on MHC-I orient toward the A-pocket, forming hydrogen bonds with the N-terminal NH. Consequently, this arrangement results in the thiol of the cysteine residue being exposed to the solvent.

Using the DLGAP5-SCT, we then investigated the probe through dose- and time-dependent labeling experiments. Both in-gel fluorescence and ELISA assays indicated that within the concentration range tested (1-100 μM), the probe exhibited increased labeling without reaching saturation (Supplementary Fig. 11a, b). Since the cell-impermeable sulfonated maleimide probes are non-toxic (Supplementary Fig. 2c), for future experiments, higher probe concentrations could potentially provide broader coverage of labeled antigen cysteines. For labeling kinetics, our results showed that 50 μM of MS-DTB achieved the highest labeling after 5–10 min (Supplementary Fig. 11b), consistent with the rapid kinetics of the maleimide moiety in cysteine labeling[40].

Harnessing cysteines in the immunopeptidome to induce phagocytosis

Finally, we sought to demonstrate the application of this platform for targeting antigen cysteines to induce antibody-dependent cellular phagocytosis (ADCP), an immune mechanism involving Fc receptors, such as CD32, on effector cells that recognize and clear antibody-coated target cells[41]. We synthesized a bifunctional molecule, M-Fc-III-4C (Fig. 7a), by conjugating a maleimide moiety to Fc-III-4C, an Fc-binding cyclic peptide[42], via a PEG linker. Fc-III-4C binds to a region of the Fc domain of human immunoglobulin G (IgG) that is distinct from the Fc receptor binding site[42], making it a suitable component for Antibody Recruiting Molecules (ARMs) designed to recruit immune cells such as macrophages and natural killer (NK) cells[43]. To evaluate M-Fc-III-4C, we used a Jurkat-Luc NFAT-CD32 cell model, which features an NFAT-inducible luciferase reporter gene activated by the Fc receptor CD32 upon encountering antibody-coated cells (Fig. 7b, c). We treated MT2 parental, *HLA* partial knockout, and *HLA* complete knockout cells with M-Fc-III-4C, washed away unbound compound, and then co-cultured the labeled cells with Jurkat-Luc NFAT-CD32 cells in the presence of human IgG (Fig. 7d). ADCP was observed with MT2 parental cells, whereas a significant decrease in ADCP was noted in MT2 *HLA* knockout cells (Fig. 7e). These results suggest that the ADCP induced by M-Fc-III-4C is likely partially mediated by reactive cysteines on MHC-I-bound antigens. Although the promiscuous maleimide moiety in M-Fc-III-4C is likely reactive with multiple cysteines on MHC-I-bound antigens and surface proteins, this proof-of-concept experiment highlights the potential of targeting antigen cysteines to manipulate cell functions and develop therapeutics.

Discussion

In this study, we introduce a platform that employs cell-impermeable cysteine-reactive probes to map reactive cysteines on MHC-I-bound antigens. We found that cysteines on MHC-I-bound antigens may exhibit various degrees of reactivity. This variability may stem from their positions on antigens and the unique conformations adopted by individual pMHC-I complexes. These conformational differences could affect the pKa value of cysteines, resulting in variations in their reactivity. Harnessing cysteine reactivity is a fundamental strategy in covalent drug and chemical probe discovery[8]. Our findings suggest potential opportunities for targeting reactive cysteines on MHC-I antigens with electrophilic small molecules or biomolecules, thereby reshaping pMHC-I complexes on the cell surface for therapeutic interventions. Furthermore, oxidative stress has been shown to promote the generation of post-translational neoantigens, influencing antigen-specific immunity dynamics[44]. For example, viral infection communicates with cytotoxic T cells through the *S*-glutathionylation occurring on the cysteines of MHC-I-presented viral peptides[45]. Our platform has the potential to map these changes in cysteines within the MHC-I immunopeptidome, providing crucial insights into antitumor and antiviral immune responses.

Recent studies have demonstrated a unique mechanism for covalent drugs capable of hijacking antigen presentation pathways, resulting in the presentation of haptenated neoepitopes on MHC-I[10,11]. Antibodies targeting these chemical neoantigens can be developed and integrated into BiTEs to recruit cytotoxic T cells. A fundamental question following these studies is: what other electrophilic small molecules have the potential to generate these chemical neoantigens? Our platform can facilitate the discovery of these molecules in various ways. First, the compatibility of sulfonated maleimide probes in ELISA assays enables the high-throughput measurement of small molecules, biomolecules, and physiological conditions that could induce the formation of chemical neoantigens by hindering the engagement of sulfonated maleimide probes within pMHC-I complexes. Second, utilizing sulfonated maleimide probes in immunopeptidomics and reactivity-based antigen profiling provides a way to identify the sequences of these chemical neoantigens.

Nonetheless, we recognize the limitations of this initial platform. One limitation is that sulfonated maleimide probes do not label MHC-I-bound antigens exclusively. They can also label MHC-II-bound antigens and a small fraction of extracellular proteins containing the reduced form of cysteines in specific physiological contexts. Therefore, at the current stage, incorporating a pairwise cellular model with *HLA* knockout and integrating a T cell epitope prediction algorithm to retain only the top-ranked MHC-I-bound peptides would be advantageous in narrowing down the observed effect to MHC-I-associated antigens.

Finally, we propose that coupling small molecules targeting antigen cysteines with secondary moieties – such as CD3-binding single-chain variable fragments (scFvs) for T cells or antibody recruitment modules for NK cells and macrophages – could offer therapeutic benefits. The main challenge is identifying selective covalent engagers of antigen cysteines that are preferentially presented on tumor cells. Nonetheless, with over 20,000 cysteine-containing MHC-I-bound peptide antigens listed in IEDB, this presents a valuable research opportunity. Our study provides an initial framework for identifying reactive cysteines that are more prevalent or exclusive in tumor cells compared to normal cells. By employing strategies such as phage display[46] and mRNA display[47], it is possible to develop cell-impermeable, peptide-based binders that selectively target pMHC-I antigen cysteines. These selective binders could be used to create bifunctional molecules that recruit immune cells for therapeutic applications.

Methods

Reagents

The anti-FLAG HRP antibody (clone M2, cat#: A8592) and anti-FLAG affinity gel (clone M2, cat#: A2220) were purchased from Sigma-Aldrich. The anti-β-Actin antibody (clone#: C4, cat#: sc-47778) was purchased from Santa Cruz Biotechnology. Streptavidin-HRP (cat#: 3999), anti-GAPDH (clone 14C10, cat#: 3683), anti-MHC Class I (clone EMR8-5, cat#: 88274) and anti-PSMB9 (clone E7J1L, cat#: 87667) antibodies were purchased from Cell Signaling Technology. The anti-hCD20-hIgG2 (clone Rituximab: anti-hCD20-hIgG2, kappa, cat#: hcd20-mab2) and anti-β-Gal-hIgG2 (monoclonal, cat#: bgal-mab2) antibodies were purchased from InvivoGen. Puromycin (cat#: ant-pr-1) was purchased from InvivoGen. InVivoMAb anti-human MHC Class I (*HLA-A*, *HLA-B*, *HLA-C*) (clone W6/32, cat#: BE0079) for ELISA assay was purchased from Bio X Cell. Ultra-LEAF anti-human *HLA-A,B,C* antibody (clone W6/32, cat#: 311448) for immunopeptidomics was purchased from BioLegend. Human IgG isotype (cat#: 31154) was purchased from Thermo Scientific. Polyethylenimine (PEI, MW 40,000, cat#: 24765-1) was purchased from Polysciences, Inc. Tetramethylrhodamine (TAMRA) azide (cat#: T10182), enzyme-linked chemiluminescence (ECL) (cat#: 32106) western blotting detection reagents, QuantaBlu fluorogenic peroxidase substrate kit (cat#: 15169), Streptavidin agarose (cat#: 20349), Streptavidin-FITC (cat#: 11-4317-87), *HLA-A,B,C* FITC antibody (clone W6/32, cat# MA5-44095), beta-2-microglobulin HRP (clone B2M-01, cat#: MA1-19679), and Tandem Mass Tag (TMT) isobaric label reagent (cat#: 90066 for TMTsixplex and cat#90406 for TMT10plex) were purchased from Thermo Scientific. FuGene 6 (cat#: E2692) transfection reagent and sequencing grade modified trypsin (cat#: V5111) were purchased from Promega. Cas9 endonuclease was purchased from Integrated DNA Technologies. pMHC-I-*HLA-A2*-KRAS-G12C was purchased from ProImmune. Maleimide-sulfonate-dibenzocyclooctyne (MSD), Maleimide-dibenzocyclooctyne (MD), Maleimide-sulfonate-PEG4-dibenzocyclooctyne (MSD4), and N-hydroxysuccinimide (NHS)-sulfonate-biotin were purchased from BroadPharm.

Cell lines

HEK293T and MDA-MB-231 cells were obtained from ATCC. BV173 cells were obtained from CLS Cell Lines Service. MT2 cells were obtained from Thermo Scientific. Jurkat-Lucia NFAT-CD32 cells and Raji cells were obtained from InvivoGen. HEK293T and MDA-MB-231 cells were cultured in Dulbecco's Modified Eagle Medium (DMEM, Corning) with 10% (v/v) fetal bovine serum (FBS, Omega Scientific) and L-glutamine (2 mM, Gibco). BV173, MT2 and Raji cells were cultured in RPMI 1640 (Corning) with 10% (v/v) FBS (Omega Scientific) and L-glutamine (2 mM, Gibco). Jurkat-Lucia NFAT-CD32 cells were cultured in Iscove's Modification of DMEM (Corning) with 10% (v/v) FBS (Omega Scientific). All the cell lines were tested negative for mycoplasma contamination.

Generation of CRISPR-Cas9-mediated *HLA* knockout cells

BV173, MT2 and MDA-MB-231 cells with *HLA-A,B,C* CRISPR-Cas9 knockout were generated through electroporation of Cas9-sgRNA ribonucleoprotein (RNP) complex using 4D-Nucleofector (Lonza Bioscience). Three sgRNAs targeting *HLA* gene (*HLA* sgRNA#1: CGGCTACTACAACCAGAGCG; *HLA* sgRNA#2: AGATCACACTGAC CTGGCAG; *HLA* sgRNA#3: AGGTCAGTGTGATCTCCGCA) were mixed for the electroporation.

Cloning and mutagenesis

Human KRAS4A-G12C cDNAs with N-terminal FLAG tag and all single-chain trimers were purchased as gene block from Integrated DNA Technologies and cloned into pCDH-CMV-MCS-EF1-Puro vector via NehI and BamHI sites. pp65 mutants were generated using Q5 site-directed mutagenesis kit (New England Biolabs).

Generation of KRAS4A-G12C stably expressed cells

Lentivirus containing FLAG-KRAS4A-G12C were generated by co-transfection of FLAG-KRAS4A-G12C, psPAX2 and pMD2.G into HEK293T cells using FuGene 6 transfection reagent. Medium containing lentiviral particles were collected 48 h post transfection, filtered with 0.45 μM Millex-HV sterile syringe filter unit (MilliporeSigma), and used to transduce BV173 cells in the presence of 10 μg/mL polybrene. 48 h post transduction, puromycin (2 μg/mL) was added and incubated with the cells for 7 days.

Cell lysis and Western blot

Cells were lysed utilizing radioimmunoprecipitation assay (RIPA) lysis buffer (Thermo Scientific) comprising 25 mM Tris-HCl, pH 7.6, 150 mM NaCl, 1% Nonidet P40 (NP-40), 1% sodium deoxycholate, and 0.1% sodium dodecyl sulfate (SDS). Before usage, the lysis buffer was supplemented with the cOmplete protease inhibitor cocktail (Roche). The cell suspension underwent sonication through 5 cycles at 40% power for 4 pulses each. Subsequent to sonication, the resultant mixture underwent centrifugation at 16,000 *g* for 10 min at 4 °C to acquire the supernatant. The protein concentration in the supernatant was determined employing the DC assay (Bio-Rad). The protein lysate was combined with Laemmli sample buffer (Bio-Rad) and heated at 95 °C for 5 min. Proteins were analyzed using 4–20% Novex Tris-Glycine mini gels (Invitrogen), followed by transfer onto a 0.2 μM polyvinylidene fluoride (PVDF) membrane (Bio-Rad). The PVDF membrane was incubated with 5% non-fat milk in Tris-buffered saline with Tween 20 (TBST) buffer (0.1% Tween 20, 20 mM Tris-HCl at pH 7.6, and 150 mM NaCl) for 1 hour at room temperature. Primary antibodies were diluted in 5% non-fat milk in TBST buffer and incubated with the membrane. Incubation durations were 1 h at room temperature for FLAG and β-actin, and overnight at 4 °C for others. Following primary antibody incubation, the membrane underwent three washes with TBST buffer and was then incubated with a secondary antibody (diluted 1:5000 in 5% non-fat milk in TBST) for 1 h at room temperature. After three additional washes with TBST buffer, the chemiluminescence signal on the membrane was developed using ECL Western blotting detection reagent, and the resultant signal was captured using ChemiDoc MP (Bio-Rad).

Immunoprecipitations

Cells were lysed in NP-40 lysis buffer (25 mM Tris-HCl, pH 7.4, 150 mM NaCl, 10% glycerol, 1% NP-40) supplemented with complete protease inhibitor cocktail. The cell suspension was incubated on ice for 10 min. Following this, the mixture was centrifuged at 16,000 *g* for 10 min at 4 °C, and the resulting supernatant was collected for use in immunoprecipitation. For immunoprecipitation, FLAG affinity gel (25 μL slurry per sample) was added to the protein lysates and rotated at 4 °C for 2 h. The affinity gel was then washed four times with immunoprecipitation washing buffer comprising 0.2% NP-40, 25 mM Tris-HCl at pH 7.4, and 150 mM NaCl. Subsequently, the affinity gel was mixed with Laemmli sample buffer and heated at 95 °C for 10 min. The resulting supernatant, containing the eluted proteins, was collected and utilized for subsequent western blot analysis.

Global proteomics

For global proteomics comparing MT2 WT and *HLA* partial KO cells, two biological replicates were used for each group. For comparisons between MT2 WT and *HLA* complete KO cells, MDA-MB-231 WT and *HLA* KO cells, and BV173 WT and *HLA* KO cells, three biological replicates were used for each group. Cells were lysed in 100 μL of PBS using sonication (10 pulses at 40% intensity, 3 rounds). Protein concentration was determined via a DC assay. Next, 100 μg of proteins in 100 μL of lysis buffer were denatured with 8 M urea. For reduction, 5 μL of 200 mM dithiothreitol (DTT) stock solution in water was added, and the mixture was heated to 65 °C for 15 min. Alkylation was achieved by

adding 5 μL of 400 mM iodoacetamide stock solution in water and incubating in the dark at 37 °C for 30 min. Proteins were then precipitated by adding 600 μL of methanol, 200 μL of chloroform, and 500 μL of water. After precipitation, protein pellets were washed with 1 mL of methanol. The resulting protein pellets were solubilized in 160 μL of 4-(2-hydroxyethyl)piperazine-1-propanesulfonic acid (EPPS) buffer (200 mM). Subsequently, 2 μg of LysC was added to each sample, and digestion was carried out at 37 °C for 2 h. This was followed by the addition of 5 μg of trypsin to each sample for another round of digestion, allowed to proceed at 37 °C for 12 h. For TMT labeling, 12.5 μg of resulting peptides in 35 μL of EPPS buffer were utilized. To each sample, 9 μL of acetonitrile was added, followed by TMT tags (3 μL per sample). The samples were then incubated at room temperature for 1 hour. The TMT labeling reaction was quenched by adding 6 μL of a 5% hydroxylamine solution, followed by the addition of 2.5 μL of formic acid. The samples were pooled and separated into 12 distinct fractions using the Thermo Vanquish Ultra High-Performance Liquid Chromatography (UHPLC) fractionator. These fractions were analyzed on an Orbitrap Eclipse Tribrid mass spectrometer coupled with a Vanquish Neo UHPLC system. Peptides were injected onto an EASY-Spray HPLC column (C18, 2 μm particle size, 75 μm inner diameter, 250 mm length) and eluted at a flow rate of 0.25 μL/min, following a gradient: 5% buffer B (80% acetonitrile with 0.1% formic acid) in buffer A (water with 0.1% formic acid) from 0 to 15 min, 5% to 45% buffer B from 15 to 155 min, and 45% to 100% buffer B from 155 to 180 min. The parameters for the MS1 scan are: resolution 120,000, *m/z* range 375–1600, RF lens 30%, standard automatic gain control (AGC) target and auto maximum injection time. In the MS2 analysis, precursor ions were quadrupole-isolated (isolation window 0.7) and then subjected to higher-energy collisional dissociation (HCD) collision in the ion trap (standard AGC, collision energy 30%, maximum injection time 35 ms). Following each MS2 spectrum, synchronous precursor selection (SPS) enabled the selection of 10 MS2 fragment ions for MS3 analysis. These MS3 precursors were fragmented by HCD and analyzed using the Orbitrap (collision energy 55%, AGC 250%, maximum injection time 200 ms, resolution 60,000). The RAW data was analyzed using Proteome Discoverer 2.5. Cysteine residues were searched with a static modification for carbamidomethylation (+57.0215). Methionine residues were searched with a dynamic modification for oxidation (+15.9949). Lysine residues and peptide N-termini were searched with a static modification for TMT labeling (+229.1629). MS3 quantification was performed with 6-plex or 10-plex TMT analysis parameters (6-plex: *m/z* 126.127725, 127.12476, 128.134433, 129.131468, 130.141141 and 131.138176; 10-plex: m/z 126.127726, 127.124761, 127.131081, 128.128116, 128.134436, 129.131471, 129.13779, 130.134825, 130.141145 and 131.13818) with a mass tolerance of 30 ppm. Protein relative abundance was calculated based on the corresponding MS3 intensity.

Cysteine-directed ABPP

For cysteine-directed ABPP that measures proteome-wide cysteine engagement by MS-DTB in cell lysates or live cells, and cysteine-directed ABPP that identifies cysteine-containing peptides directly enriched by IA-DTB, MS-DTB, or MSD-DTB, two biological replicates were used for each group. Cells were lysed in PBS via sonication (10 pulses at 40% intensity, 3 rounds). The protein concentration was determined using a DC assay and adjusted to 1 mg/mL. Next, 500 μL of lysates were labeled with 100 μM IA-DTB, DBIA, MS-DTB or MSD-DTB at room temperature for 1 h. Protein precipitation was achieved by adding 500 μL of methanol and 100 μL of chloroform, followed by a methanol wash (1 mL). The resulting protein pellets were denatured using 90 μL of 9 M urea and 10 mM DTT in 50 mM tetramethylammonium bicarbonate. Alkylation was carried out using 50 mM iodoacetamide at 37 °C for 30 min. Subsequently, 350 μL of 50 mM tetramethylammonium bicarbonate was added to each sample, followed by the addition of 2 μg of trypsin. Digestion was allowed to proceed at 37 °C for 12 h. Next, 50 μL of streptavidin-agarose beads were added to each sample, and the mixture was rotated at room temperature for 2 h. The beads were washed three times with 1 mL of washing buffer consisting of 0.2% NP-40, 25 mM Tris-HCl pH 7.4, and 150 mM NaCl, followed by three washes with 1 mL of PBS, and two washes with 1 mL of water. Peptides were eluted using 300 μL of 50% acetonitrile containing 0.1% formic acid. The eluted peptides were subsequently dried using a SpeedVac vacuum concentrator. The subsequent steps of TMT labeling and LC-MS analysis were carried out following the methodology described in global proteomics. During RAW data analysis, cysteine residues were searched with a dynamic modification for carbamidomethylation (+57.0215), IA-DTB (455.2744), DBIA (296.1848), MS-DTB (690.2894), hydrolyzed MS-DTB (708.3000), MSD-DTB (992.4062) or hydrolyzed MSD-DTB (1010.4168).

Immunopeptidomics

For immunopeptidomics, two biological replicates were used for each group. 2×10^8 BV173 or MT2 cells were lysed using 3 mL of lysis buffer (0.5% NP-40, 50 mM Tris pH 8.0, 150 mM NaCl, 1 mM ethylenediaminetetraacetic acid (EDTA), and protease inhibitor cocktail) by rotating at 4 °C for 30 min. Following centrifugation at 18,000 *g* for 10 min, the supernatant was collected for enrichment using an anti-MHC antibody (W6/32, BioLegend) conjugated to Affi-gel 10 matrix (Bio-Rad, 2 mg of antibody per 100 μL of slurry per sample). Enrichment occurred over 4 h of rotation at 4 °C, followed by transfer to a Bio-spin column (Bio-Rad) for washing with 3 × 1 mL of lysis buffer, wash buffer 1 (50 mM Tris pH 8, 150 mM NaCl), wash buffer 2 (50 mM Tris pH 8, 400 mM NaCl), and wash buffer 3 (50 mM Tris pH 8). MHC-conjugated peptides were subsequently eluted using 1 mL of 1% trifluoroacetic acid in water. Peptide samples were desalted using a Sep-Pak C18 cartridge (Waters), dried via speedavac, and analyzed using an Orbitrap Eclipse Tribrid mass spectrometer coupled with a Vanquish Neo UHPLC system. The subsequent step LC-MS analysis was carried out following the methodology described in global proteomics. Motif analysis of peptides was performed using the Seq2Logo method[48].

Reactivity-based antigen profiling

For probe enrichment experiments, two biological replicates were used for each group. 10^8 cells were treated with 50 μM of MS-DTB for 30 min. After treatment, the cells were washed twice with PBS and then harvested. Subsequently, the cells were lysed in 5 mL of lysis buffer containing 2 M urea and 0.2% NP-40 in PBS using sonication (10 pulses at 40% intensity, 3 rounds). Following centrifugation at 18,000 *g* for 10 min, the supernatant was collected for enrichment using streptavidin agarose beads. The mixture was rotated at room temperature for 2 h. The beads were then washed three times with 1 mL of washing buffer (0.2% NP-40, 25 mM Tris-HCl pH 7.4, and 150 mM NaCl), followed by three washes with 1 mL of wash buffer 1 (50 mM Tris pH 8, 150 mM NaCl), wash buffer 2 (50 mM Tris pH 8, 400 mM NaCl), PBS, and water. Peptides were eluted using 300 μL of 50% acetonitrile containing 0.1% formic acid. The eluted peptides were subsequently dried using a SpeedVac vacuum concentrator and desalted using a Sep-Pak C18 cartridge. The peptides were analyzed using an Orbitrap Eclipse Tribrid mass spectrometer coupled with a Vanquish Neo UHPLC system. The subsequent step LC-MS analysis was carried out following the methodology described in global proteomics.

Modeling study

The crystal structures of *HLA-A**02:01 (2X4R) and *HLA-A**24:02 (2BCK) from Protein Data Bank (X-ray structures with a resolution finer than 3.5 Å), $KRAS^{G12C}$ neoantigen (KLVVVGACGV) and three MS-DTB-enriched antigens: CTDSP2 (CYVKDLSRL), DLGAP5 (RYRPDMPCF), and CCR8 (CYIKILHQL) were used for the modeling study. MHC-Fine, a refined AlphaFold model, was used for MHC-peptide complex

prediction[49]. The final PDB files of the MHC-peptide complex were generated by running the inference code and datasets (https://bitbucket.org/abc-group/mhc-fine/src/main/). The figures were generated by PyMOL software. For each MHC protein, only the α1 and α2 domains were used.

The FASTA sequence of *HLA-A**02:01: GSHSMRYFFTSVSRPGRGEPRFIAVGYVDDTQFVRFDSDAASQRMEPRAPWIEQEGPEYWDGETRKVKAHSQTHRVDLGTLRGYYNQSEAGSHTVQRMYGCDVGSDWRFLRGYHQYAYDGKDYIALKEDLRSWTAADMAAQTTKHKWEAAHVAEQLRAYLEGTCVEWLRRYLENGKETLQRT

The FASTA sequence of *HLA-A**24:02: GSHSMRYFSTSVSRPGRGEPRFIAVGYVDDTQFVRFDSDAASQRMEPRAPWIEQEGPEYWDEETGKVKAHSQTDRENLRIALRYYNQSEAGSHTLQMMFGCDVGSDGRFLRGYHQYAYDGKDYIALKEDLRSWTAADMAAQITKRKWEAAHVAEQQRAYLEGTCVDGLRRYLENGKETLQRT

Cell surface probe labeling by flow cytometry

Cells were seeded in non-treated 6-well plates and treated with 50 μM of reactivity probes for 30 min. Following treatment, cells were rinsed with PBS and suspended in flow cytometry buffer (1 mM EDTA, 25 mM HEPES pH 7.0, 1% FBS in PBS) within Eppendorf tubes. Subsequently, Streptavidin-FITC or *HLA-A,B,C*-FITC antibody (diluted 1:50) was added, and the cells were rotated at room temperature for 30 min. Afterward, the cells were washed with PBS and resuspended in flow cytometry buffer. FITC fluorescence on the cell surface was quantified using a BD LSRFortessa Cell Analyzer, and the resulting data were analyzed utilizing FlowJo software.

LC-MS analysis of probe-peptide adduct

Peptides were synthesized by GenScript. 100 μM peptide and 100 μM compound were incubated in water for 30 min and analyzed by Thermo Vanquish UHPLC coupled to ISQ EC Single Quadrupole Mass Spectrometer. Peptide and probe-peptide adduct were separated on Gemini C18 column (Phenomenex, 5 μm, 50 × 4.6 mm) at a flow rate of 1 mL/min, following the gradient: 0 to 95% buffer C (acetonitrile with 0.1% formic acid) in buffer A (water with 0.1% formic acid) from 0 to 13 min, and 95% buffer C in buffer A from 13 to 20 min. 210 nm wavelength was used to monitor the peaks. A full scan from *m/z* 200-1250 with positive mode was used to analyze unmodified peptide and probe-peptide adduct. Two biological replicates were used for each group.

ELISA assay

Nunc MaxiSorp 384-well plates (black) were coated overnight with 50 μL of the anti-heavy chain antibody W6/32 at a concentration of 5 μg/mL in PBS. Following coating, the plates were washed twice with PBS (100 μL) and blocked with 3% bovine serum albumin (BSA) in PBS (120 μL) at room temperature for 1 h. Subsequently, the plates were washed three times with 0.05% Tween-20 in PBS (PBST) (100 μL each wash). BV173, MT2 parental, and *HLA* knockout cells were treated with 50 μM of MS-DTB for 30 min, then harvested and lysed in NP-40 lysis buffer with protease inhibitor cocktail. The protein concentration was adjusted to 1 mg/mL, and 50 μL of total lysates were added to each well. Plates were incubated at 4 °C for 4 h, followed by three washes with 1% BSA in PBS (100 μL each wash). Next, 50 μL of either 1 μg/mL anti-beta-2-microglobulin HRP conjugate solution or Streptavidin-HRP (diluted 1:1000) in 1% BSA PBS was added to each well. Plates were incubated with shaking at room temperature for 1 h. The plates were washed three times with PBST and three times with PBS (100 μL each wash). 50 μL of the HRP substrate QuantaBlu was added, and fluorescence was measured using the CLARIOstar Plus microplate reader (BMG Labtech).

In-gel fluorescence

HEK293T cells were transfected with SCTs using PEI transfection reagent. Following a 24 h incubation, the cells were treated with 50 μM of MSD for 30 min. Subsequently, cells were harvested by centrifugation at 500 *g* for 5 min and then lysed in NP-40 lysis buffer containing protease inhibitor cocktail. The resulting lysate was subjected to immunoprecipitation with anti-Flag affinity gel at 4 °C for 2 h. The affinity gel was washed three times with immunoprecipitation washing buffer and re-suspended in 18 μL of PBS. For the click chemistry reaction, the following reagents were added: 0.8 μL of 1.5 mM TAMRA azide solution in DMSO, 1.2 μL of 10 mM Tris(benzyltriazolylmethyl)amine solution in 4:1 tBuOH:DMSO, 1 μL of 40 mM $CuSO_4$ solution in H_2O, and 1 μL of 40 mM Tris(2-carboxyethyl)phosphine solution in H_2O. The reaction proceeded at room temperature for 1 h. Subsequently, Laemmli sample buffer was added and heated at 95 °C for 10 min. Following centrifugation at 15,000 *g* for 2 min, the supernatant was collected, and the samples were resolved by 4–20% Novex Tris-Glycine mini gels. In-gel fluorescence signals were recorded using the Chemi-Doc MP system.

Cell viability assay

Cells were plated in a 96-well clear bottom white plate (Corning) at a density of 5000 cells per well in 100 μL of DMEM medium and incubated for 24 h. Subsequently, the cells were treated with varying concentrations of compounds in 100 μL of DMEM medium for additional 72 h. Following treatment, 50 μL of Cell Titer Glo reagent (Promega) was added to each well and incubated for 10 min at room temperature. Luminescence was measured using CLARIOstar Plus microplate reader (BMG Labtech).

Antibody-dependent cellular phagocytosis assay

For the assay with Raji cells, 90 μL of Raji cells in RPMI (1.1×10^5 cells per well) were added in 96-well plate in the presence of 20 μL anti-hCD20-hIgG2 (5 μg/mL) or anti-β-Gal-hIgG2 (10 μg/mL). After 1 h incubation, Raji cells were co-cultured with Jurkat-Luc NFAT-CD32 cells (2.2×10^5 cells per well). The mixture was then incubated at 37 °C for 8 h. 20 μL of the cultured supernatant was transferred to a 96-well white plate and mixed with 50 μL of QUANTI-Luc Lucia 4 (InvivoGen) per well. The luciferase activity was measured using CLARIOstar Plus microplate reader. For the assay targeting reactive cysteines of MHC-I-bound antigens in MT2 cells, MT2 wildtype and *HLA* knockout cells were treated with DMSO or M-Fc-III-4C (10 μM) in serum free RPMI medium for 30 min. After washing with PBS to remove free compound, 90 μL of cell suspension (1.1×10^5 cells per well) were added in 96-well plate in the presence of 20 μL of human IgG isotype control (5 μg/mL). MT2 cells were subsequently co-cultured with Jurkat-Luc NFAT-CD32 cells (2.2×10^5 cells per well). The mixture was incubated at 37 °C for 8 h. 20 μL of the cultured supernatant was transferred to a 96-well white plate and mixed with 50 μL of QUANTI-Luc Lucia 4 (InvivoGen) per well. The luciferase activity was measured using CLARIOstar Plus microplate reader.

Statistical analysis

Quantitative data were depicted using scatter plots, displaying the mean accompanied by the standard error of the mean (SEM) represented as error bars. Differences between two groups were assessed using an unpaired two-tailed Student's *t*-test. Significance levels were denoted as follows: $^*P < 0.05$, $^{**}P < 0.01$, $^{***}P < 0.001$, and ns, not significant. Statistical significance was defined for P values < 0.05.

Reporting summary

Further information on research design is available in the Nature Portfolio Reporting Summary linked to this article.

Data availability

The data supporting the findings of this study are available within the article and Supplementary Information. The mass spectrometry proteomics data have been deposited to the ProteomeXchange

Consortium via the PRIDE[50] partner repository with the dataset identifier PXD054678. Source data of all uncropped gels and blots are provided in the Source Data file. *P* values are included in the Source Data file. The protein structures were retrieved from the Protein Data Bank with the accession codes: 2X4R; 2BCK. Source data are provided with this paper.

Code availability

The code for the MHC-peptide complex modeling study is available on Bitbucket: https://bitbucket.org/abc-group/mhc-fine/src/main/.

References

1. Hansen, T. H. & Bouvier, M. MHC class I antigen presentation: learning from viral evasion strategies. *Nat. Rev. Immunol.* **9**, 503–513 (2009).
2. Fernando, M. M. et al. Defining the role of the MHC in autoimmunity: a review and pooled analysis. *PLoS Genet* **4**, e1000024 (2008).
3. Schumacher, T. N. & Schreiber, R. D. Neoantigens in cancer immunotherapy. *Science* **348**, 69–74 (2015).
4. Trowsdale, J. The MHC, disease and selection. *Immunol. Lett.* **137**, 1–8 (2011).
5. Raskov, H., Orhan, A., Christensen, J. P. & Gogenur, I. Cytotoxic CD8(+) T cells in cancer and cancer immunotherapy. *Br. J. Cancer* **124**, 359–367 (2021).
6. Dendrou, C. A., Petersen, J., Rossjohn, J. & Fugger, L. HLA variation and disease. *Nat. Rev. Immunol.* **18**, 325–339 (2018).
7. Palafox, M. F., Desai, H. S., Arboleda, V. A. & Backus, K. M. From chemoproteomic-detected amino acids to genomic coordinates: insights into precise multi-omic data integration. *Mol. Syst. Biol.* **17**, e9840 (2021).
8. Boike, L., Henning, N. J. & Nomura, D. K. Advances in covalent drug discovery. *Nat. Rev. Drug Discov.* **21**, 881–898 (2022).
9. Szeto, C. et al. Covalent TCR-peptide-MHC interactions induce T cell activation and redirect T cell fate in the thymus. *Nat. Commun.* **13**, 4951 (2022).
10. Hattori, T. et al. Creating MHC-Restricted Neoantigens with Covalent Inhibitors That Can Be Targeted by Immune Therapy. *Cancer Discov.* **13**, 132–145 (2023).
11. Zhang, Z. et al. A covalent inhibitor of K-Ras(G12C) induces MHC class I presentation of haptenated peptide neoepitopes targetable by immunotherapy. *Cancer Cell* **40**, 1060–1069 e1067 (2022).
12. Yi, M. C. & Khosla, C. Thiol-Disulfide Exchange Reactions in the Mammalian Extracellular Environment. *Annu Rev. Chem. Biomol. Eng.* **7**, 197–222 (2016).
13. Vinogradova, E. V. et al. An Activity-Guided Map of Electrophile-Cysteine Interactions in Primary Human T Cells. *Cell* **182**, 1009–1026 e1029 (2020).
14. Kuljanin, M. et al. Reimagining high-throughput profiling of reactive cysteines for cell-based screening of large electrophile libraries. *Nat. Biotechnol.* **39**, 630–641 (2021).
15. Caldwell, S. T. et al. Photoactivated release of membrane impermeant sulfonates inside cells. *Chem. Commun. (Camb.)* **57**, 3917–3920 (2021).
16. Juanes, M., Lostale-Seijo, I., Granja, J. R. & Montenegro, J. Supramolecular Recognition and Selective Protein Uptake by Peptide Hybrids. *Chemistry* **24**, 10689–10698 (2018).
17. Kolb, H. C., Finn, M. G. & Sharpless, K. B. Click Chemistry: Diverse Chemical Function from a Few Good Reactions. *Angew. Chem. Int Ed. Engl.* **40**, 2004–2021 (2001).
18. Jewett, J. C. & Bertozzi, C. R. Cu-free click cycloaddition reactions in chemical biology. *Chem. Soc. Rev.* **39**, 1272–1279 (2010).
19. Jacobs, A. T. & Marnett, L. J. Systems analysis of protein modification and cellular responses induced by electrophile stress. *Acc. Chem. Res.* **43**, 673–683 (2010).
20. McConnell, E. W., Smythers, A. L. & Hicks, L. M. Maleimide-based chemical proteomics for quantitative analysis of cysteine reactivity. *J. Am. Soc. Mass Spectrom.* **31**, 1697–1705 (2020).
21. Gonzalez-Galarza, F. F., Christmas, S., Middleton, D. & Jones, A. R. Allele frequency net: a database and online repository for immune gene frequencies in worldwide populations. *Nucleic Acids Res.* **39**, D913–D919 (2011).
22. Scholtalbers, J. et al. TCLP: an online cancer cell line catalogue integrating HLA type, predicted neo-epitopes, virus and gene expression. *Genome Med.* **7**, 118 (2015).
23. Nusinow, D. P. et al. Quantitative Proteomics of the Cancer Cell Line Encyclopedia. *Cell* **180**, 387–402 e316 (2020).
24. Stryhn, A. et al. pH dependence of MHC class I-restricted peptide presentation. *J. Immunol.* **156**, 4191–4197 (1996).
25. Poole, L. B. & Nelson, K. J. Discovering mechanisms of signaling-mediated cysteine oxidation. *Curr. Opin. Chem. Biol.* **12**, 18–24 (2008).
26. Kacen, A. et al. Post-translational modifications reshape the antigenic landscape of the MHC I immunopeptidome in tumors. *Nat. Biotechnol.* **41**, 239–251 (2023).
27. Purcell, A. W., Ramarathinam, S. H. & Ternette, N. Mass spectrometry-based identification of MHC-bound peptides for immunopeptidomics. *Nat. Protoc.* **14**, 1687–1707 (2019).
28. Tadros, D. M., Eggenschwiler, S., Racle, J. & Gfeller, D. The MHC Motif Atlas: a database of MHC binding specificities and ligands. *Nucleic Acids Res.* **51**, D428–D437 (2023).
29. Kawamura, K. et al. Development of a Unique T Cell Receptor Gene-Transferred Tax-Redirected T Cell Immunotherapy for Adult T Cell Leukemia. *Biol. Blood Marrow Transpl.* **26**, 1377–1385 (2020).
30. Neefjes, J., Jongsma, M. L., Paul, P. & Bakke, O. Towards a systems understanding of MHC class I and MHC class II antigen presentation. *Nat. Rev. Immunol.* **11**, 823–836 (2011).
31. Ferrington, D. A. & Gregerson, D. S. Immunoproteasomes: structure, function, and antigen presentation. *Prog. Mol. Biol. Transl. Sci.* **109**, 75–112 (2012).
32. Zhou, F. Molecular mechanisms of IFN-gamma to up-regulate MHC class I antigen processing and presentation. *Int Rev. Immunol.* **28**, 239–260 (2009).
33. Hansen, T., Yu, Y. Y. L. & Fremont, D. H. Preparation of stable single-chain trimers engineered with peptide, beta2 microglobulin, and MHC heavy chain. *Curr. Protoc. Immunol.* 17 15 11-17 15 17 (2009).
34. Greten, T. F. et al. Peptide-beta2-microglobulin-MHC fusion molecules bind antigen-specific T cells and can be used for multivalent MHC-Ig complexes. *J. Immunol. Methods* **271**, 125–135 (2002).
35. Yu, Y. Y., Netuschil, N., Lybarger, L., Connolly, J. M. & Hansen, T. H. Cutting edge: single-chain trimers of MHC class I molecules form stable structures that potently stimulate antigen-specific T cells and B cells. *J. Immunol.* **168**, 3145–3149 (2002).
36. Linette, G. P., Bear, A. S. & Carreno, B. M. Facts and hopes in immunotherapy strategies targeting antigens derived from KRAS mutations. *Clin. Cancer Res.* **30**, 2017–2024 (2024).
37. Kula, T. et al. T-Scan: A Genome-wide Method for the Systematic Discovery of T Cell Epitopes. *Cell* **178**, 1016–1028 e1013 (2019).
38. Backus, K. M. et al. Proteome-wide covalent ligand discovery in native biological systems. *Nature* **534**, 570–574 (2016).
39. Unanue, E. R., Turk, V. & Neefjes, J. Variations in MHC Class II Antigen Processing and Presentation in Health and Disease. *Annu Rev. Immunol.* **34**, 265–297 (2016).
40. Ravasco, J., Faustino, H., Trindade, A. & Gois, P. M. P. Bioconjugation with Maleimides: A Useful Tool for Chemical Biology. *Chemistry* **25**, 43–59 (2019).
41. Tay, M. Z., Wiehe, K. & Pollara, J. Antibody-Dependent Cellular Phagocytosis in Antiviral Immune Responses. *Front Immunol.* **10**, 332 (2019).

42. Sasaki, K. et al. Fc-binding antibody-recruiting molecules exploit endogenous antibodies for anti-tumor immune responses. *Chem. Sci.* **11**, 3208–3214 (2020).
43. McEnaney, P. J., Parker, C. G., Zhang, A. X. & Spiegel, D. A. Antibody-recruiting molecules: an emerging paradigm for engaging immune function in treating human disease. *ACS Chem. Biol.* **7**, 1139–1151 (2012).
44. Kroemer, G., Galassi, C., Zitvogel, L. & Galluzzi, L. Immunogenic cell stress and death. *Nat. Immunol.* **23**, 487–500 (2022).
45. Trujillo, J. A. et al. The cellular redox environment alters antigen presentation. *J. Biol. Chem.* **289**, 27979–27991 (2014).
46. Hamzeh-Mivehroud, M., Alizadeh, A. A., Morris, M. B., Church, W. B. & Dastmalchi, S. Phage display as a technology delivering on the promise of peptide drug discovery. *Drug Discov. Today* **18**, 1144–1157 (2013).
47. Josephson, K., Ricardo, A. & Szostak, J. W. mRNA display: from basic principles to macrocycle drug discovery. *Drug Discov. Today* **19**, 388–399 (2014).
48. Thomsen, M. C. & Nielsen, M. Seq2Logo: a method for construction and visualization of amino acid binding motifs and sequence profiles including sequence weighting, pseudo counts and two-sided representation of amino acid enrichment and depletion. *Nucleic Acids Res.* **40**, W281–W287 (2012).
49. Glukhov, E. et al. MHC-Fine: Fine-tuned AlphaFold for Precise MHC-Peptide Complex Prediction. 2023.2011.2029.569310 (2023).
50. Perez-Riverol, Y. et al. The PRIDE database resources in 2022: a hub for mass spectrometry-based proteomics evidences. *Nucleic Acids Res.* **50**, D543–D552 (2022).

Acknowledgements

We gratefully acknowledge the support of the Ono Pharma Foundation (X.Z.) and NIH T32 GM149439 (A.M.). We thank the Robert H. Lurie Comprehensive Cancer Center of Northwestern University for the use of the Flow Cytometry Core Facility.

Author contributions

C.Zhang, C.Zhou and X.Z. conducted biochemical and cellular experiments; C.Zhang synthesized MSD-DTB, MS-DTB and M-Fc-III-4C, and conducted the modeling study and reporter assays; C.Zhou and X.J. conducted ELISA assays; C.Zhang, A.M., and X.Z. conducted the proteomics and immunopeptidomics studies and performed data analysis; D.F. provided guidance on studies related to MT2 cells; X.Z. supervised the project and, with contributions from all authors, wrote the manuscript.

Competing interests

The authors declare no competing interests.

Additional information

Supplementary information The online version contains supplementary material available at https://doi.org/10.1038/s41467-024-54139-8.

Correspondence and requests for materials should be addressed to Xiaoyu Zhang.

Peer review information *Nature Communications* thanks Charles S Craik, Hiroyuki Katayama, Anthony Purcell and the other, anonymous, reviewer(s) for their contribution to the peer review of this work. A peer review file is available.